CHALMERS
UNIVERSITY OF TECHNOLOGY

Active Air Suspension Modeling and Control for Roll Stability in Heavy-duty Vehicles

Master's thesis in Systems, Control and Mechatronics

Samuel Lee
Jakob Olson

DEPARTMENT OF ELECTRICAL ENGINEERING
CHALMERS UNIVERSITY OF TECHNOLOGY
Gothenburg, Sweden 2025
www.chalmers.se

Master's thesis 2025

Active Air Suspension Modeling and Control for Roll Stability in Heavy-duty Vehicles

Samuel Lee
Jakob Olson

CHALMERS
UNIVERSITY OF TECHNOLOGY

Department of Electrical Engineering
Chalmers University of Technology
Gothenburg, Sweden 2025

Active Air Suspension Modeling and Control for Roll Stability in Heavy-duty Vehicles
Samuel Lee
Jakob Olson

Supervisor: Maliheh Sadeghi Kati, VOLVO TECHNOLOGY AB
Supervisor: Esteban Gelso, VOLVO TECHNOLOGY AB
Examiner: Jonas Fredriksson, Department of Electrical Engineering, Chalmers

Master's Thesis 2025
Department of Electrical Engineering
Chalmers University of Technology
SE-412 96 Gothenburg
Telephone +46 31 772 1000

Cover: Simulated heavy truck during a high-speed turn

Typeset in LaTeX
Printed by Chalmers Reproservice
Gothenburg, Sweden 2025

Active Air Suspension Modeling and Control for Roll Stability in Heavy-duty Vehicles

Samuel Lee
Jakob Olson

Department of Electrical Engineering
Chalmers University of Technology

Abstract

Heavy-duty trucks are particularly vulnerable to rollovers during aggressive manoeuvres due to their high centre of gravity and large, often unevenly distributed mass. Traditional passive suspension systems cannot often actively counteract rollovers. This thesis examines the application of active air suspension controlled by a Nonlinear Model Predictive Controller (NMPC) to improve roll stability by leveraging future steering information.

A high-fidelity multibody truck model, based on the Volvo Transport Model (VTM), was extended to include active suspension dynamics. Nonlinear vehicle dynamics were modelled to accurately capture the coupled interactions between longitudinal, lateral, vertical, roll and yaw dynamics for the use in the NMPC. The controller was implemented using CasADi and integrated within a MATLAB/Simulink framework. It utilized the FATROP solver to predict future vehicle states and optimally adjust suspension forces to mitigate roll motion while maintaining the desired speed.

The controller was deployed and tested against a baseline controller in various driving scenarios. Simulation results demonstrate that the controller consistently reduces lateral load transfer and roll angle for rollover-prone driving scenarios. The controller has demonstrated the ability to prevent rollovers by actively using the vertical forces in the air-suspension system for realistic driving scenarios. However, the system also showed limitations in handling fast alternating maneuvers, such as lane changes.

The findings suggest that integrating active suspension with predictive control can improve the dynamic stability and safety of heavy-duty trucks.

Keywords: Nonlinear Model Predictive Control, Vehicle Dynamics, Active Air Suspension, Roll Stability, Rollover Prevention, Optimal Control, Modelling, Heavy Vehicle, Longitudinal Dynamics, Lateral Dynamics, Vertical Dynamics.

Acknowledgements

We want to extend our thanks to our supervisors at Volvo GTT, Maliheh Sadeghi Kati and Esteban Gelso for their continuous support during our thesis. You have been very helpful and pedagogical. Without your input this would not be possible.

We would also like to thank our examiner at Chalmers, Professor Jonas Fredriksson. Thank you for your feedback and material provided during our thesis.

Finally a big thanks to all of Volvo GTT and all very helpful employees at VMM for assisting us and paying an interest to our thesis. Thank you for the high quality computers and supportive environment. Lastly a special thank you Nrupathunga Ashok for your valuable knowledge of suspensions and Berk Varol for the time you took to assist us during this thesis.

Samuel Lee, Gothenburg, May 2025
Jakob Olson, Gothenburg, May 2025

List of Acronyms

Below is the list of acronyms that have been used throughout this thesis, listed in alphabetical order:

COG	Center of Gravity
FATROP	Fast Real-Time Optimization Solver
LTR	Lateral Load Transfer Ratio
MPC	Model Predictive Control
NMPC	Nonlinear Model Predictive Control
ODE	Ordinary Differential Equation
PI	Proportional-Integral (Controller)
RK4	Runge-Kutta 4th Order (Numerical Integration Method)
VTM	Volvo Transport Model
ZOH	Zero Order Hold

Nomenclature

Below is the nomenclature of indices, parameters and variables that have been used throughout this thesis.

Indices

i	Index for tire-suspension units ($i = 1, \ldots, 6$)
k	Discrete time step index in NMPC horizon
t	simulation time

Parameters

A_{ef}	Effective area of air spring
A_f	Frontal area of the truck
b	Critical pressure ratio for air
C_d	Aerodynamic drag coefficient
C_{rr}	Rolling resistance coefficient
C_z	Vertical damping coefficient of suspension (Extended VTM)
$C_{z,vtm}$	Vertical damping coefficient of suspension (Original VTM)
C_r	Roll damping coefficient (Extended VTM)
F_0	Initial suspension force
g	Gravitational constant
h_{roll}	Height from roll center to COG
I_{xx}, I_{yy}, I_{zz}	Moments of inertia for roll, pitch, and yaw axes respectively
K_z	Vertical suspension stiffness (Extended VTM)
$K_{z,vtm}$	Vertical Suspension Stiffness (Original VTM)
$K_{z,bump}$	Vertical stiffness from bumper
$K_{z,m2m}$	Vertical metal to metal stiffness

K_r	Roll stiffness (Extended VTM)
$K_{r,ar}$	Roll stiffness contribution from anti-roll bar
$K_{r,aux}$	Roll stiffness contribution from auxiliary springs
l_f, l_m, l_r	Longitudinal distance from COG to front, middle, rear axles
L	Total wheelbase of the truck
m	Total vehicle mass
m_{axle}	Weight of all axles
n	Polytropic coefficient
N	Prediction horizon
P_{atm}	Atmospheric pressure
P_0	Initial spring pressure
P_{tank}	Tank pressure
Q, R	NMPC weight matrices for states and inputs
R	Specific gas constant for air
T_s	Sampling time of controller/Temperature of air inside air spring
$\dot{T}_s$	Air Temperature Rate in Air spring
V_0	Initial spring volume
γ	Specific heat ratio of air
η	Drivetrain efficiency
r	Wheel radius
s	Valve orifice area
w_{sf}, w_{sm}, w_{sr}	Spring lateral distance for each axle
w_{damp}	Dampers lateral distance
w_{tf}, w_{tm}, w_{tr}	Track width for front, middle, and rear axles
z_{bump}	Bumper stiffness distance threshold
z_{m2m}	Metal to metal stiffness distance threshold

Variables

F_x, F_y, F_z	Total longitudinal, lateral, and vertical forces
F_{xi}, F_{yi}, F_{zi}	Forces at tire i in longitudinal, lateral, and vertical directions
$F_{zs,i}$	Vertical suspension force at suspension i
F_{drag}	Aerodynamic drag force
F_{roll}	Rolling resistance force

v_x, v_y	Longitudinal and lateral velocity
ϕ, $\dot{\phi}$, $\ddot{\phi}$	Roll angle and roll rate, roll acceleration
ψ, $\dot{\psi}$, $\ddot{\psi}$	Yaw angle, yaw rate, yaw acceleration
δ	Steering angle
δ_{ref}	Reference steering angle
P_s	Air spring pressure
V_s	Air spring volume
p_u	Upstream Pressure
p_d	Downstream Pressure
$\dot{V}_s$	Air spring volume change
$\dot{P}_s$	Rate of change of air spring pressure
m_s	Mass of air in the spring
$\dot{m}_s$	Mass flow rate into/out of the air spring
z, $\dot{z}$	Suspension displacement and velocity
u	Control input vector
x	State vector
x_{ref}	Reference state vector
J	Objective function of NMPC
α_i	Tire slip angle at wheel i
M_Z	Total yaw moment
K_{us}	Understeer gradient
$\Delta\bar{F}_z$	Lateral load transfer ratio

Contents

List of Figures

List of Tables

1

Introduction

1.1 Background

Heavy-duty vehicles, such as trucks, are prone to instability, including rollovers, during challenging maneuvers, sharp turns, or lane changes. A rollover is when a vehicle loses contact with the ground on one side and tips over. This is primarily due to the high centre of gravity, large mass, and non-uniform weight distribution. In 1997, the Swedish parliament introduced Nollvisionen (Vision Zero) [1]. Nollvisionen establishes that the long-term goal is that no one should be killed or seriously injured within the road transport system. Rollover crashes are rare but disproportionately deadly, comprising only 2.2% of all motor vehicle crashes yet accounting for 33% of injury-related costs and nearly one-third of all highway vehicle occupant fatalities in the U.S [2]. In addition to the high risk of severe injury or death, rollover events also impose significant economic burdens, including vehicle downtime, cargo damage, and emergency response costs [2].

To enhance ride comfort and axle load leveling, most modern trucks already feature air suspension systems. These systems typically operate in a passive manner, adjusting ride height but not actively counteracting dynamic forces. As such, they are not used to suppress the lateral load transfer that leads to rollovers.

However, the presence of air suspension provides an opportunity. By controlling the pressure in each suspension, it is theoretically possible to influence the vehicle's behaviour. If this control is made active rather than reactive, it might reduce the risk of rollover by generating counteracting suspension forces during critical maneuvers.

Recent developments in artificial intelligence have enabled progress in the field of path prediction. Machine learning models based on deep learning can successfully predict possible future paths of the target vehicles and generate a multimodal solution [3]. This capability enables a controller to preview the prediction horizon and treat the steering input as a known predictable disturbance, allowing the controller to anticipate lateral forces and dynamically adjust the suspension system accordingly.

This motivates a more advanced air suspension model that accounts for its dynamics and interaction with vehicle roll. Such a model can then be used to explore

advanced predictive control strategies that aim to improve vehicle stability.

1.2 Problem Statement

The problem is to design a control strategy that can anticipate roll in advance and actively manage suspension forces to mitigate roll. The challenge lies in developing a controller that can handle the fast and nonlinear vehicle dynamics, as well as the relatively slow suspension system dynamics.

1.3 Objectives

To investigate the problem statement, the following objectives have been defined:

- Extend an existing high-fidelity vehicle dynamics model, Volvo Transport Model (VTM), to include active air suspension and all necessary interfaces for control integration for system validation purposes.
- Develop a vehicle dynamics model capturing longitudinal, lateral, vertical, roll, and yaw behaviour suitable for control design.
- Formulate and implement a predictive controller to apply optimal suspension forces to reduce the risk of rollover.
- Evaluate the system's performance across different scenarios to assess controller performance.

1.4 Limitations of Scope

Since this thesis focuses on the development and simulation of a predictive controller for active suspension to mitigate rollovers, several limitations are considered:

- Simulation-only validation: The controller is evaluated only in a simulation environment based on VTM. No hardware or experimental validation is performed.
- Assumed preview information: Future steering angles are assumed to be known, which may not be directly available in a real-world implementation without additional sensor systems or prediction mechanisms. There is no observer, all states are assumed available.
- Neglected road and environmental variability: Effects such as varying road friction, uneven surface, or load shifts due to cargo movement are not explicitly modelled, yielding a simpler model.
- Real-time performance: The controller is not intended for real-time deployment, and the computational performance is not investigated in this study.

1.5 Thesis Structure

The thesis begins by detailing the multibody modeling with air suspension, to extend the VTM model configuration, Chapter 2. This is followed by Chapter 3, which

outlines the modeling of a nonlinear vehicle model suitable for control design, including longitudinal, lateral, vertical, yaw, and roll behaviors. Chapter 4 shows the control design and presents the formulation and implementation of NMPC, including limits, constraints, and tuning. Finally, Chapter 5 presents simulation results and discussion evaluating the controller's performance under critical driving scenarios. Chapter 6 concludes the contributions of the thesis and outlines potential directions for future work.

2

Multibody Modeling with Air Suspension

This chapter details the development of a multi-body vehicle model of an air suspension system. It begins with the Vehicle Transport Model (VTM), which is extended kinematically to incorporate air suspension, thereby enabling the simulation of vertical and roll dynamics. The extended model is validated through simulations. The chapter then covers air suspension modeling, including the physics of air springs, a nonlinear model of pressure-force dynamics, and a mass flow rate model for air exchange. Finally, these components are integrated into the VTM simulation framework.

2.1 Volvo Transport Model

The VTM is an internally developed, complete heavy vehicle model that can be easily adapted to represent a wide range of vehicle configurations. The model is built using Simscape and Simulink and has been validated through real-life tests and data [4]. The purpose of the VTM model is to test and develop control architecture, crash reconstruction, and driving simulations.

The model consists of rigid bodies representing the cab, axles, and multiple rigid bodies to account for frame torsion. The tire dynamics used are the Magic Tire Formula [5]. The roll dynamics of the VTM model consist of a roll center and a translational joint for each axle stiffness, as shown in Figure 2.1. The stiffnesses and damping coefficients have been calculated to account for the effects of the anti-roll bars, dampers, springs, and auxiliary springs, creating a realistic vehicle model.

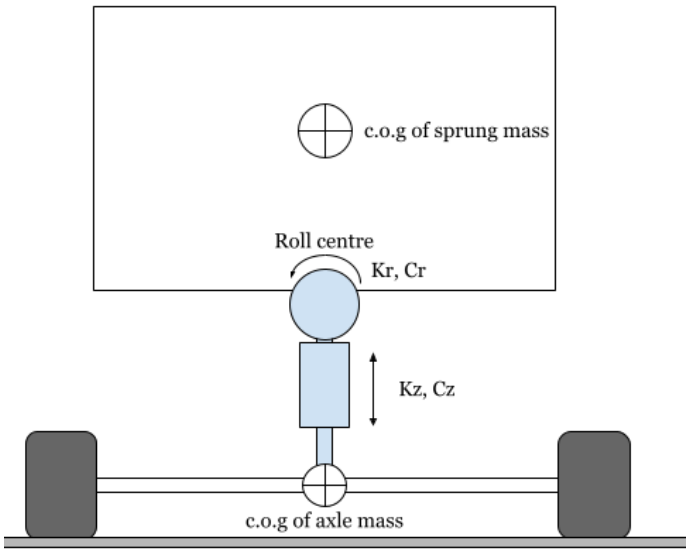

Figure 2.1: VTM suspension kinematic configuration

2.1.1 Kinematic Extension of the VTM Model

To account for differences in ride height between the left and right sides of the suspension when modeling roll dynamics using a roll center, the suspension model's degrees of freedom must be expanded. Instead of using a single translational and rotational degree of freedom per axle, as seen in Figure 2.1, each side needs to be modeled with an independent translational degree of freedom. This is implemented using two prismatic joints, each with associated stiffness and damping laterally offset from the original suspension installation position, as shown in Figure 2.2.

Because rotational motion does not directly correspond to translational motion, two auxiliary rotational degrees of freedom are introduced at each end of the prismatic joints. These are modelled using rotational joints without stiffness or damping. The upper rotational joint is vertically aligned with the roll centre, while the lower one is aligned with the wheel's ground contact point and connected to the axle's sprung mass.

The lower joint is placed at the wheel-ground contact point, rather than directly below the axle, to accommodate cases where the roll centre lies below the axle. Placing the joint too high could lead to an unstable configuration. While this arrangement may seem unintuitive, it enables modelling of asymmetric ride heights. To ensure Simscape can simulate the system, two negligible intermediary bodies with small mass and inertia are introduced between the auxiliary joints.

The setup provides the necessary degrees of freedom to represent differing left-right ride heights. The complete kinematic configuration of the suspension is illustrated in Figure 2.2.

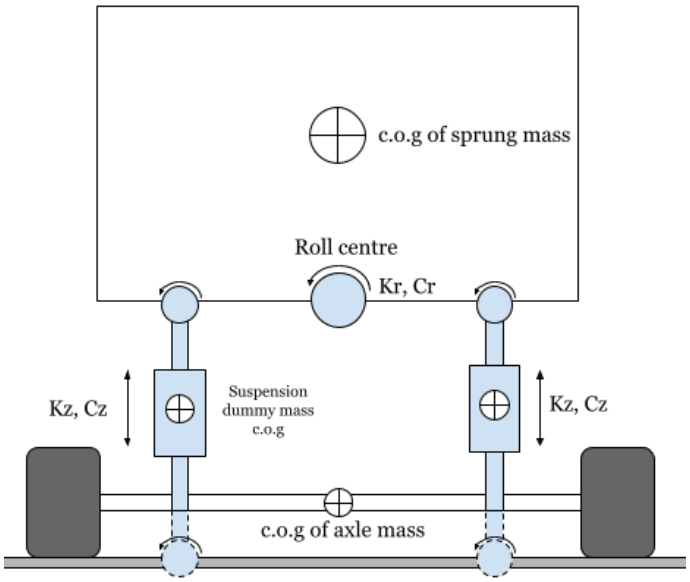

Figure 2.2: Extended VTM Simscape suspension kinematic configuration

The new vertical stiffness for the translational joints, K_z and C_z, are simply defined as follows:

$$K_z = \frac{K_{z,vtm}}{2}, \quad C_z = \frac{C_{z,vtm}}{2} \tag{2.1}$$

where $K_{z,vtm}$ is the original VTM vertical stiffness and $C_{z,vtm}$ is the vertical damping coefficient. The total roll stiffness, K_r , excluding the vertical spring stiffness K_z, is given by:

$$K_r = K_{r,\text{ar}} + K_{r,\text{aux}} \tag{2.2}$$

where $K_{r,\text{ar}}$ is the roll stiffness from the anti-roll bar, and $K_{r,\text{aux}}$ is the roll stiffness from the auxiliary spring configuration. As the dampers are installed farther from the roll centre than the springs, the roll damping is adjusted accordingly:

$$C_r = 2C_z \left(w_{\text{damp}}^2/2 - w_{\text{spring}}^2/2 \right) \tag{2.3}$$

where w_{damp} and w_{spring} are the lateral distances of the dampers and springs from the roll centre, respectively. The parameters used are taken internally from Volvo Trucks and will therefore not be disclosed in the report.

2.1.2 Validation of Kinematic Extension of the VTM Model

To validate the new kinematic configuration, the proposed model is compared to the original configuration through simulation. The simulated scenario is a 50-meter radius turn at a speed of 7.07 m/s. The roll and pitch of the frontmost center of gravity are nearly identical and can be seen in Figures 2.3 and 2.4, respectively.

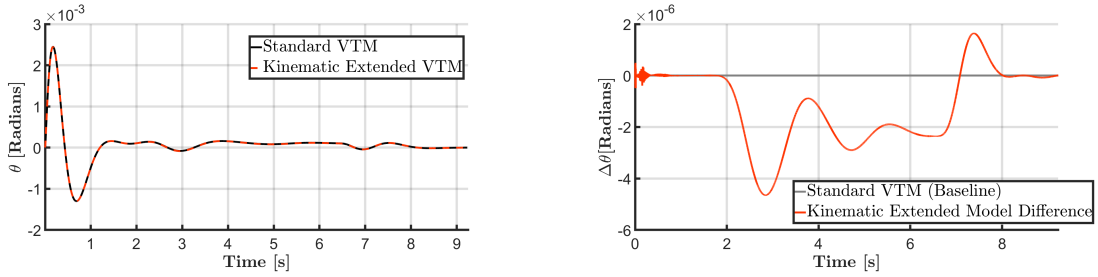

(a) Pitch **(b)** Pitch Difference

Figure 2.3: Comparison of Pitch between Original VTM and Kinematic Extended VTM model

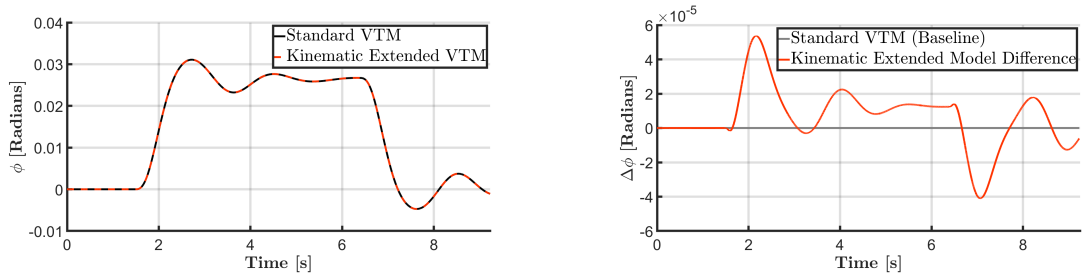

(a) Roll **(b)** Roll Difference

Figure 2.4: Comparison of Roll between Original VTM and Kinematic Extended VTM model

There are small deviations of the mean difference for roll and pitch, $\mu_{e,roll}$ and $\mu_{e,pitch}$,

$$\mu_{e,roll} = 6.25 \cdot 10^{-6} \qquad \mu_{e,pitch} = -1.14 \cdot 10^{-6} \tag{2.4}$$

The small deviations can most likely be attributed to the dummy masses and small angles of the auxiliary rotational joints. This demonstrates that the kinematically extended model closely replicates the behaviour of the original VTM model, but with added degrees of freedom for the suspension.

2.2 Air Suspension Modelling

A vehicle's suspension system is designed to ensure a smooth ride and provide optimal handling conditions for the tires. In heavy-duty vehicles, such as those used for freight transport, air springs are often used in place of traditional mechanical springs. This preference is due to several inherent advantages offered by air springs, such as adjustable load-carrying capacity, adjustable ride height, reduced weight, and variable stiffness characteristics [6].
Among the various types of air springs, this thesis focuses on the bellow-type air spring, as illustrated in Figure 2.5. This type of spring operates by inflating a flexible, elastic membrane, known as the bellow, to a pressure higher than the surrounding atmospheric pressure, thereby generating a counteracting upward force.

Within the bellow, there is a bumper to protect the mechanical parts, for instance, in the scenario of depressurization of the bellow.

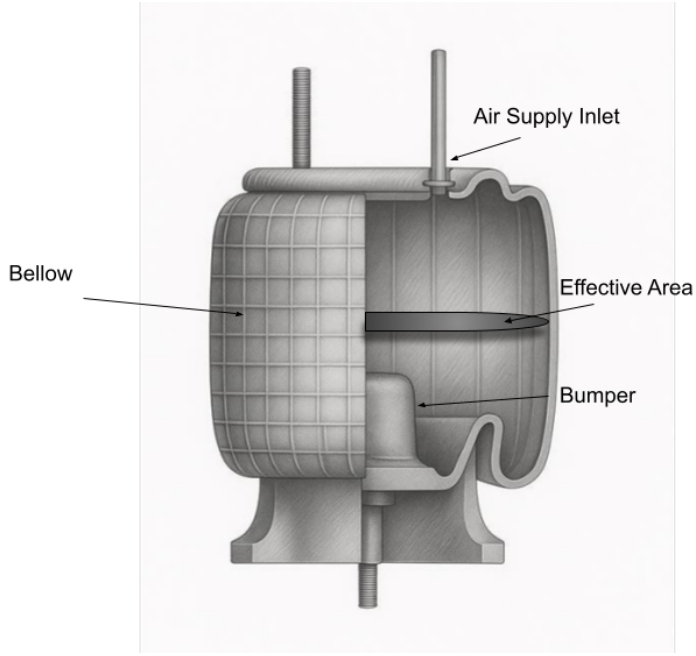

Figure 2.5: Illustration of bellow type air spring, [7]

.

Similar to mechanical springs, the force generated by an air spring increases with compression, i.e, displacement. This is primarily due to the reduction in internal volume during compression, which results in an increase in pressure.

Air springs are typically connected to an air supply system, often consisting of one or more compressed air tanks. A control valve regulates airflow into the bellow, increasing internal pressure and, consequently, the spring force and stiffness. Conversely, another valve vents air to the atmosphere to reduce the internal pressure when needed.

2.2.1 Air Spring Pressure and Force Modelling

In [8], the dynamic behaviour of the pressure within an air spring is derived from the ideal gas law as:

$$\dot{P}_s = \frac{P_s}{T_s}\dot{T}_s + \frac{RT_s}{V_s}\dot{m}_s - \frac{P_s}{V_s}\dot{V}_s \tag{2.5}$$

where P_s is the internal pressure of the air spring, T_s is the internal temperature, V_s is the volume of the bellow, R is the specific gas constant for air, and $\dot{m}_s$ is the mass flow rate into or out of the bellow. The resulting vertical force from the air spring can be computed as follows, [8, 9]:

$$F = (P_s - P_{\text{atm}})A_{\text{ef}} \tag{2.6}$$

where F is the vertical force, P_{atm} is atmospheric pressure, and A_{ef} is the approximated constant effective area of the bellow.

Since the thesis focuses on evaluating vehicle and controller performance with air springs, certain assumptions are made to simplify the model. First, the temperature inside the air spring is assumed constant, i.e., $\dot{T}_s = 0$. Additionally, the volume of the bellow is assumed to vary linearly with vertical displacement z, as motivated by the experimental results in [10], which report that the relationship between air spring volume and height is nearly linear. This leads to the following expressions for bellow volume, V_s and volume rate $\dot{V}_s$:

$$\begin{aligned} V_s &= V_0 - zA_{\text{ef}} \\ \dot{V}_s &= -\dot{z}A_{\text{ef}} \end{aligned} \tag{2.7}$$

where V_0 is the initial bellow volume, z is the vertical displacement, and $\dot{z}$ is the vertical velocity. The displacement is defined as positive when the spring is compressed and negative when it expands. Under these assumptions, (2.5) simplifies to:

$$\dot{P}_s = \frac{RT_s}{V_0 - zA_{\text{ef}}}\dot{m}_s - \frac{P_s A_{\text{ef}}}{V_0 - zA_{\text{ef}}}\dot{z} \tag{2.8}$$

This expression describes how the pressure changes with respect to the mass flow rate, displacement, and displacement velocity. In the scenario when there are two air springs per side and axle, the effective area and volumes of the springs are added together.
An additional factor that must be considered is the preload of the springs, the initial force they must exert to balance the static load. This preload determines the pressure required from the system to reach equilibrium with the gravitational force acting on the sprung mass. The initial force balance is given by:

$$\begin{aligned} F_0 &= \frac{m_a g}{2} = (P_0 - P_{atm})A_{ef} \\ \rightarrow P_0 &= \frac{m_a g}{2A_{ef}} + P_{atm} \end{aligned} \tag{2.9}$$

where m_a is the sprung mass load on each axle, g the gravitational constant and P_0 the initial pressure.

2.2.2 Mass Flow Rate Modelling

To model the air mass flow rate, [11] provides formulations for flow through a solenoid on/off valve based on whether the flow is choked or unchoked:

$$\dot{m}_s = \begin{cases} s\frac{p_u}{\sqrt{RT_s}}\sqrt{\gamma\left(\frac{2}{\gamma+1}\right)^{\frac{\gamma+1}{\gamma-1}}}, & 0 < \frac{p_d}{p_u} \leq b \\ \\ s\sqrt{\frac{2}{RT_s}}\sqrt{p_d(p_u - p_d)}, & b < \frac{p_d}{p_u} \leq 1 \end{cases} \tag{2.10}$$

where s is the valve's effective flow area, p_u is the upstream pressure, p_d is the downstream pressure, γ is the polytropic index, and b is the critical pressure ratio for air. Using this formulation, the mass flow rate into and out of the bellow is

described by:

$$\dot{m}_{\text{in}} = \begin{cases} s\frac{P_{\text{tank}}}{\sqrt{RT_s}}\sqrt{\gamma\left(\frac{2}{\gamma+1}\right)^{\frac{\gamma+1}{\gamma-1}}}, & 0 < \frac{P_s}{P_{\text{tank}}} \leq b \\ s\sqrt{\frac{2}{RT_s}}\sqrt{P_s(P_{\text{tank}} - P_s)}, & b < \frac{P_s}{P_{\text{tank}}} \leq 1 \end{cases}$$
$$\dot{m}_{\text{out}} = \begin{cases} -s\frac{P_s}{\sqrt{RT_s}}\sqrt{\gamma\left(\frac{2}{\gamma+1}\right)^{\frac{\gamma+1}{\gamma-1}}}, & 0 < \frac{P_{\text{atm}}}{P_s} \leq b \\ -s\sqrt{\frac{2}{RT_s}}\sqrt{P_{\text{atm}}(P_s - P_{\text{atm}})}, & b < \frac{P_{\text{atm}}}{P_s} \leq 1 \end{cases} \tag{2.11}$$

where $\dot{m}_{\text{in}}$ and $\dot{m}_{\text{out}}$ are the mass flow rates from the supply tank to the bellow and from the bellow to the atmosphere, respectively. P_{tank} is the pressure of the supply tank that is assumed constant and was chosen from experience at Volvo Trucks. Since no real-world flow data are available for direct comparison, the valve flow area s is tuned such that the vertical ride height velocity falls within the range of 10–15 mm/s, in line with recommendations based on practical experience from Volvo Trucks. The final parameter values used in the simulations are summarized in Table 2.1.

Table 2.1: Parameters of vehicle air suspension system

Parameter	**Unit**	**Value**
s	m^2	$1.76 \cdot 10^{-6}$
T_s	K	293.15
R	J/(kg·K)	287
b	Unitless	0.528
γ	Unitless	1.4
A_{ef}	m^2	Confidential
V_0	m^3	Confidential
P_{atm}	kPa	100
P_{tank}	kPa	1200
P_0	kPa	Confidential
K_z	N/m	Confidential
C_z	Ns/m	Confidential
K_r	Nm/rad	Confidential
C_r	Nms/rad	Confidential

2.3 Addition of Air Springs in VTM

To implement the air spring dynamics and flow model within the extended VTM model, each air suspension bellow is represented by a Simscape Pristmatic Joint placed on the respective sides of the multi-body configuration, replacing the vertical stiffness K_z, as shown in Figure 2.6. These joints are configured to measure the relative displacement z and velocity $\dot{z}$, which serve as inputs to both the pressure

dynamics and force calculation blocks. The air spring system for each joint can be seen in Figure 2.6.

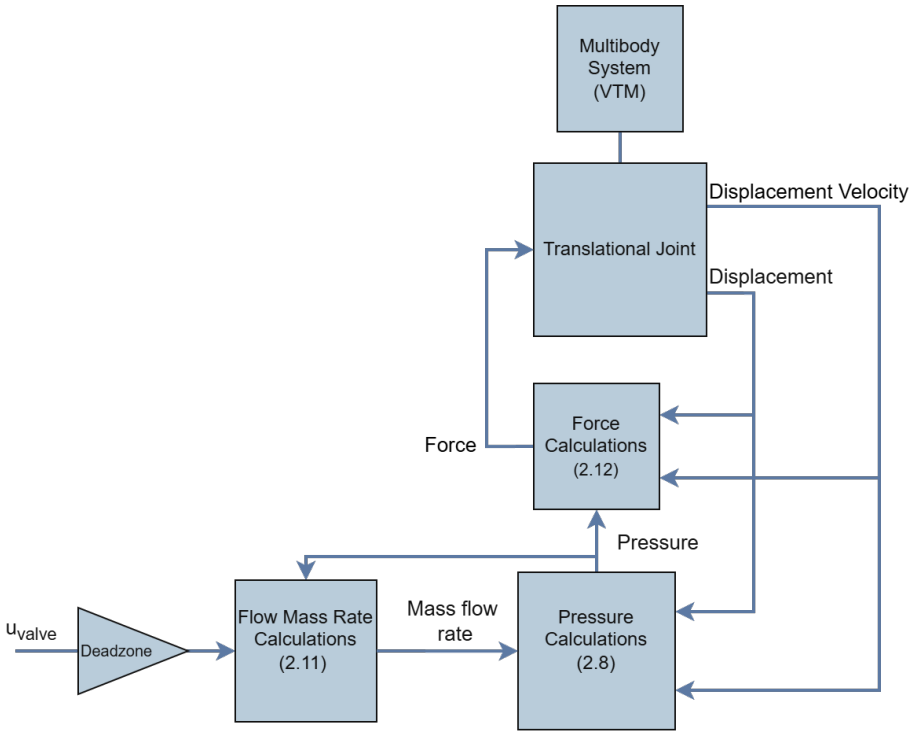

Figure 2.6: Block diagram of single air spring implementation in VTM

The pressure block uses (2.8) to compute the internal bellow pressure P_s based on z, $\dot{z}$, and the mass flow rate $\dot{m}_s$. The mass flow rate is determined using Equation (2.11), where the control input u_{valve} dictates whether the valve opens to increase or decrease pressure. To prevent oscillations when the input is near zero, a dead zone is implemented around $u_{\text{valve}} = 0$ with a threshold of 0.1, forcing the valves to close, i.e., $\dot{m}_s = 0$. Additionally, the mass flow rate calculation takes into account the current pressure P_s within the bellow.

The computed pressure P_s is then used to determine the total suspension force, which also depends on the displacement and velocity of the translational joint. The total force is calculated according to the expression in (2.12), which includes air spring force, damping, bump-stop stiffness, and metal-to-metal contact stiffness. Since the pressure model in (2.8) contains a division by $V_0 - zA_{ef}$, there is a risk of numerical instability as $V_0 - zA_{ef}$ approaches zero. To avoid division-by-zero errors and represent physical contact conditions, mechanical constraints were added to the translational joints. These include a bump-stop and a metal-to-metal contact stiffness that models the physical limitations of the suspension system.

$$F = \begin{cases} (P_s - P_{atm})A_{ef} + D_z\dot{z} & \text{, for } z < z_{bump} \\ (P_s - P_{atm})A_{ef} + D_z\dot{z} + K_{bump}z & \text{, for } z_{m2m} > z > z_{bump} \\ (P_s - P_{atm})A_{ef} + D_z\dot{z} + K_{bump}z + K_{m2m}z & \text{, for } z > z_{m2m} \end{cases} \tag{2.12}$$

where, K_{bump} and K_{m2m} represent the bump-stop and metal-to-metal stiffness coefficients, set to $10^6\,\text{N/m}$ and $10^7\,\text{N/m}$ respectively, while z_{bump} and z_{m2m} denote the corresponding displacement thresholds.

The resulting force F is applied to the translational joint, which is integrated with the rest of the VTM multibody system, including the axle and sprung mass.

3

Nonlinear Dynamics of Heavy Vehicles

In this chapter the vehicle dynamics are derived for the use in the predictive controller. The chapter begins by defining the states and control inputs in the model thereafter the equations of motion for each translational and rotational degree of freedom is derived.

3.1 Model Structure and State Selection

A two-track model represents a vehicle with separate left and right wheel tracks [12], allowing individual tire and suspension forces. This allows for accurate simulation of roll, yaw, and lateral load transfer, which is essential for capturing rollover dynamics and asymmetrical behaviour, especially in heavy vehicles with active suspension.

The model uses a vehicle-fixed coordinate system following the right-hand rule, where the x-axis points forward along the vehicle's longitudinal direction, the y-axis points to the left (lateral direction), and the z-axis points upward (normal to the ground). The state vector includes key translational and rotational dynamics relevant for stability control, as well as suspension pressure states required for modelling the active air suspension system. The state vector is defined as:

Table 3.1: State variables used in the vehicle model

State	Symbol	Description
Longitudinal velocity	v_x	Forward speed of the vehicle
Lateral velocity	v_y	Side velocity of the vehicle
Yaw angle	ψ	Heading of the vehicle about the Z-axis
Yaw rate	$\dot{\psi}$	Rate of change of yaw angle
Roll angle	ϕ	Vehicle body roll angle about X-axis
Roll rate	$\dot{\phi}$	Rate of change of roll angle
Suspension pressures	$P_1 \dots P_6$	Air spring pressures at each suspension

To design an effective predictive controller the state selection is essential, these will determine which states are tracked and controlled throughout the simulation. For this model, states were chosen in accordance to the goal of rollover prevention while still maintaining stability and control relevance.

The chosen states allow for accurate simulation of air suspension dynamics and load transfer during aggressive maneuvers. The controller model dynamics are largely derived from [12], with the extension to include three axles, detailed air suspension, and nonlinear lateral tire dynamics.

3.2 Longitudinal Vehicle Dynamics

The longitudinal dynamics of the vehicle are crucial for capturing forward motion, acceleration, and resistive forces, such as aerodynamic drag and rolling resistance. A commonly used approach for vehicle modeling is the two-track model, as illustrated below:

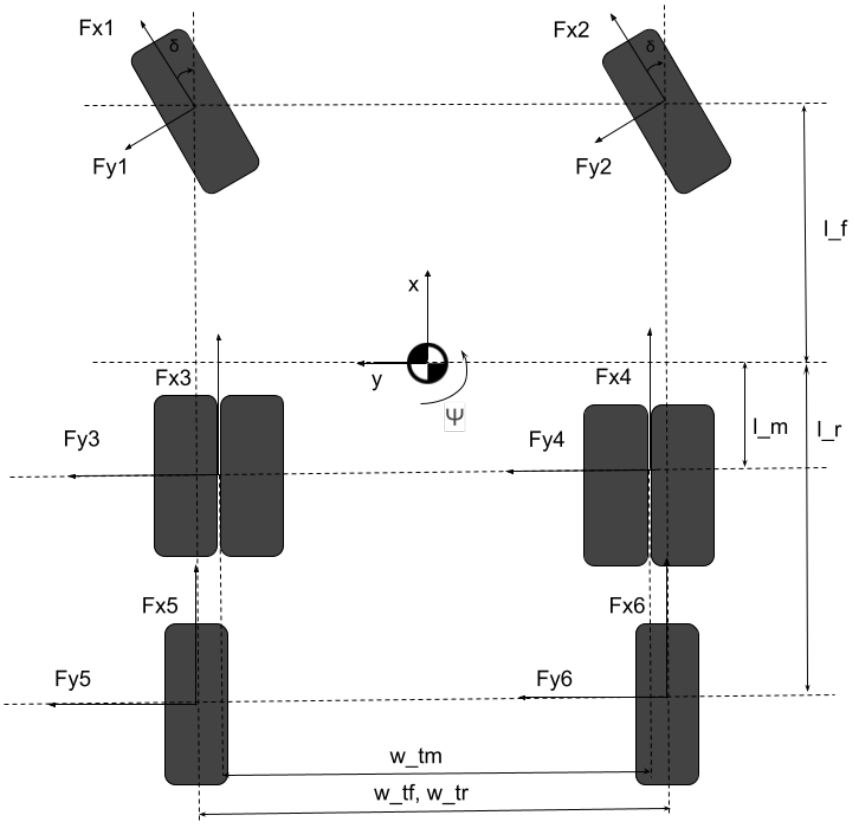

Figure 3.1: Two-track model of vehicle from top view

The time derivative of the longitudinal velocity, $\dot{v}_x$, describes how the vehicle's forward speed evolves due to applied forces and dynamic interactions. It is based on Newton's second law, with additional terms accounting for lateral motion and roll–yaw coupling effects:

$$\dot{v}_x = \frac{F_x}{m + m_{\text{axle}}} + v_y\dot{\psi} + h_{\text{roll}}\sin(\phi)\ddot{\psi} \tag{3.1}$$

where F_x represents the total longitudinal force acting on the vehicle, while m and m_{axle} denote the sprung and axle masses, respectively. The term $v_y\dot{\psi}$ captures the lateral-to-longitudinal velocity coupling due to yaw rotation. The final term, $h_{\text{roll}}\sin(\phi)\ddot{\psi}$, introduces the effect of roll-induced yaw acceleration, where h_{roll} is the distance from the roll center to the center of mass, ϕ is the roll angle, and $\ddot{\psi}$ is the yaw acceleration.

The total longitudinal force F_x acting on the truck is generated by the tires as can be seen in 3.1. For the middle axle, which has four wheels, this force is modelled as acting at a point midway between the inner and outer wheels. steering effects on the front axle, and resistive forces such as aerodynamic drag and rolling resistance:

$$F_x = F_{x1}\cos(\delta) - F_{y1}\sin(\delta) + F_{x2}\cos(\delta) - F_{y2}\sin(\delta) + F_{x3} + F_{x4} + F_{x5} + F_{x6} - F_{\text{drag}} - F_{\text{roll}} \tag{3.2}$$

where δ is the steering angle of the front wheels, and the corresponding tire forces are resolved into the longitudinal direction. Each term F_{xi} represents the longitudinal force contribution at wheel i. Only the middle axle is driven; those forces are calculated as follows:

$$F_{x3} = F_{x4} = \frac{\tau \cdot \eta}{r} \tag{3.3}$$

The motor torque, τ originates from the throttle input of the truck. It is transmitted through the drivetrain with an assumed efficiency η and converted to longitudinal force at the wheels by dividing by the wheel radius r. The aerodynamic drag force acts as a braking force on the vehicle's motion and depends on the vehicle's speed and shape:

$$F_{\text{drag}} = \frac{1}{2} C_d A \rho v_x^2 \tag{3.4}$$

where C_d is the drag coefficient, A_f is the frontal area of the vehicle, ρ is air density, and v_x is the vehicle's longitudinal velocity. The rolling resistance is modelled as a constant opposing force:

$$F_{\text{roll}} = C_{rr} m g \tag{3.5}$$

where C_{rr} is the rolling resistance coefficient, m is the sprung mass, and g is the gravitational acceleration.

3.3 Lateral Vehicle Dynamics

The lateral motion of the vehicle is primarily influenced by the lateral tire forces, which arise due to tire slip, as well as the yaw rate and steering input. Understanding these dynamics is essential for accurately capturing how the vehicle responds to directional changes.

The lateral acceleration $\dot{v}_y$ describes how the vehicle's side-to-side motion evolves, considering tire forces, yaw rate, roll effects, and inertial couplings:

$$\dot{v}_y = \frac{F_y}{m + m_{\text{axle}}} - v_x\dot{\psi} - h_{\text{roll}}\sin(\phi)\cos(\phi)\dot{\psi}^2 + h_{\text{roll}}\ddot{\phi} \tag{3.6}$$

To calculate accurate lateral tire forces, the tire slip angle α, defined as the angle between the direction a wheel is pointing and the actual direction the vehicle is moving relative to the ground, needs to be determined. It arises as the lateral velocity differs from the longitudinal velocity and often occurs in turns. The slip angles for each wheel are calculated as:

$$\alpha_1 = \tan^{-1}\left(\frac{v_y + l_f\dot{\psi}}{v_{x,\text{safe}}}\right) - \delta \qquad \text{(Front Left)} \tag{3.7}$$

$$\alpha_2 = \tan^{-1}\left(\frac{v_y + l_f\dot{\psi}}{v_{x,\text{safe}}}\right) - \delta \qquad \text{(Front Right)} \tag{3.8}$$

$$\alpha_3 = \tan^{-1}\left(\frac{v_y - l_m\dot{\psi}}{v_{x,\text{safe}}}\right) \qquad \text{(Middle Left)} \tag{3.9}$$

$$\alpha_4 = \tan^{-1}\left(\frac{v_y - l_m\dot{\psi}}{v_{x,\text{safe}}}\right) \qquad \text{(Middle Right)} \tag{3.10}$$

$$\alpha_5 = \tan^{-1}\left(\frac{v_y - l_r\dot{\psi}}{v_{x,\text{safe}}}\right) \qquad \text{(Rear Left)} \tag{3.11}$$

$$\alpha_6 = \tan^{-1}\left(\frac{v_y - l_r\dot{\psi}}{v_{x,\text{safe}}}\right) \qquad \text{(Rear Right)} \tag{3.12}$$

where l_f, l_m, l_r denote the distances from the center of gravity (COG) to the front, middle, and rear axles, respectively.

To ensure numerical stability when v_x is near zero, v_x is limited according to:

$$v_{x,\text{safe}} = \max(v_x, \varepsilon) \tag{3.13}$$

where ε is 0.1.

The lateral tire forces are computed using Pacejka's magic formula, [13], which captures the relationship between slip angle and lateral force, an important aspect under large lateral accelerations and dynamic load transfer. This method offers higher accuracy compared to linear models. However, it should be noted that the Magic Formula is not a tire model derived from physical laws, but rather it is used to empirically represent and interpolate previously measured tire force and moment curves [14]. Meaning that it approximates tire behaviour only within the range of conditions for which it has been fitted.
Given that the Magic Formula parameters are dependent on vertical load, the model to calculate each lateral tire force is defined as:

$$F_{yi} = D_i \cdot \sin\left(C \cdot \arctan\left(B_i x_i - E\left(B_i x_i - \arctan(B_i x_i)\right)\right)\right) + S_{V_i} \tag{3.14}$$

with the shifted slip angle defined as:

$$x_i = \alpha_i + S_{H_i} \tag{3.15}$$

In the expressions above, α_i denotes the slip angle at tire i, while x_i represents the effective slip angle after applying a horizontal shift S_{H_i}. The resulting lateral force is given by F_{yi}, where D_i is the peak force value, C is the shape factor, B_i is the stiffness factor, and E controls the curvature of the response near peak force. The terms S_{H_i} and S_{V_i} introduce horizontal and vertical offsets, respectively, enabling the model to more accurately replicate the asymmetric tire behavior observed in experimental data.

Since the middle axle has 2 wheels per side, the lateral forces for each side are doubled to account for this. The load-dependent formulations used for these parameters are adapted from internal Volvo resources and these specific expressions and parametrizations are considered confidential and are therefore not disclosed in full detail in this document.

To capture the effects of the lateral tire forces on the chassis, the forces are converted from the wheels to the vehicle coordinate frame and are calculated as:

$$F_y = (F_{x1}\sin(\delta)+F_{y1}\cos(\delta))+(F_{x2}\sin(\delta)+F_{y2}\cos(\delta))+F_{y3}+F_{y4}+F_{y5}+F_{y6}. \quad (3.16)$$

3.4 Roll Dynamics

The rotational dynamics of the vehicle around its longitudinal axis, typically denoted the roll dynamics, and by the roll angle ϕ. The motion is primarily influenced by lateral forces, gravitational effects, and suspension stiffness and damping. For heavy vehicles with a high centre of gravity, roll behavior is critical to safety, as excessive roll during cornering can lead to wheel lifting off the ground or rollover. Accurate modeling of roll dynamics is therefore essential for control design, especially when using active suspension to mitigate the risk of rollover.

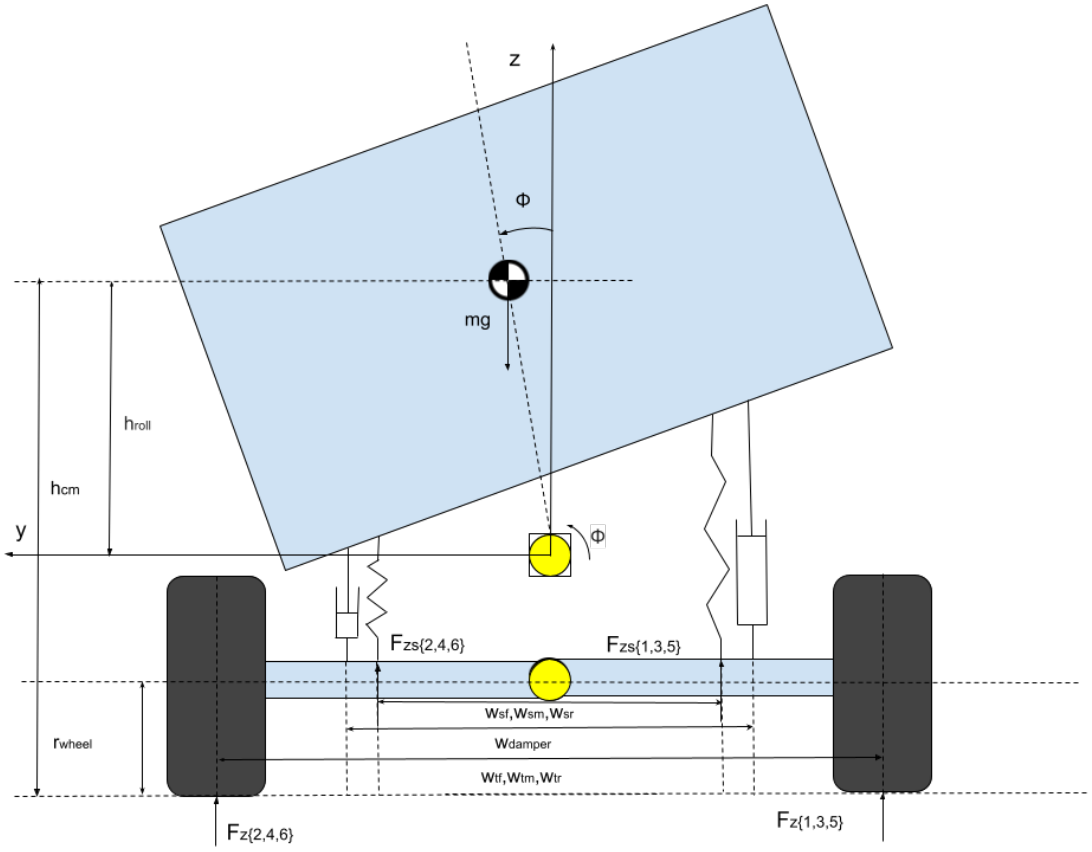

Figure 3.2: Two-track model of vehicle from front view

The roll acceleration of the vehicle body, denoted by $\ddot{\phi}$, is influenced by a balance of suspension-induced forces as described in the previous Chapter, inertial effects, and gravity. The complete expression for roll acceleration $\ddot{\phi}$ is given by:

$$\ddot{\phi} = \frac{1}{I_{xx}}\Bigg(\frac{w_{sf}}{2}(F_{zs1} - F_{zs2}) + \frac{w_{sm}}{2}(F_{zs3} - F_{zs4}) + \frac{w_{sr}}{2}(F_{zs5} - F_{zs6}) + F_y h_{\text{roll}}\cos(\phi) \\ + mgh_{\text{roll}}\sin(\phi) - K_\phi\phi - D_\phi\dot{\phi} + \dot{\psi}^2(I_{yy} - I_{zz})\sin(\phi)\cos(\phi)\Bigg) \tag{3.17}$$

where w_{sf},w_{sf} and w_{sf} spring lateral spacing for the front, middle and rear axles, F_{zi} are the suspension corner forces, F_y is the lateral force, and h_{roll} is the height from the roll centre to the COG. The terms K_ϕ and D_ϕ are the roll stiffness and damping, while $\dot{\psi}$ is the yaw rate.

3.5 Yaw Dynamics

Yaw dynamics describe the rotation of the vehicle around its vertical axis, influenced by tire-generated forces, steering input, and coupling with roll and longitudinal dynamics.

Yaw acceleration, $\ddot{\psi}$, is computed from the net yaw moment and the inertial properties of the vehicle, including coupling terms due to roll:

$$\ddot{\psi} = \frac{1}{I_{yy}\sin^2(\phi) + I_{zz}\cos^2(\phi)}\Big(M_Z + F_x h_{\text{roll}}\sin(\phi) \\ - 2(I_{yy} - I_{zz})\sin(\phi)\cos(\phi)\dot{\phi}\dot{\psi}\Big) \tag{3.18}$$

where M_Z is the net yaw moment from the tires, I_{zz} and I_{yy} represent the vehicle's moments of inertia about the pitch (lateral) and yaw (vertical) axes, and the remaining terms account for the inertial and coupling effects between roll and yaw dynamics.
The yaw moment is generated by summing the contributions of lateral and longitudinal tire forces at each wheel, scaled by their respective lever arms:

$$\begin{aligned} M_Z = {} & l_f\left(F_{y1}\cos(\delta) + F_{x1}\sin(\delta) + F_{y2}\cos(\delta) + F_{x2}\sin(\delta)\right) \\ & - l_m(F_{y3} + F_{y4}) - l_r(F_{y5} + F_{y6}) \\ & + \frac{w_{tf}}{2}\left(F_{y1}\sin(\delta) - F_{y2}\sin(\delta) - F_{x1}\cos(\delta) + F_{x2}\cos(\delta)\right) \\ & + \frac{w_{tm}}{2}(-F_{x3} + F_{x4}) + \frac{w_{tr}}{2}(-F_{x5} + F_{x6}) \end{aligned} \tag{3.19}$$

where w_{tf}, w_{tm}, and w_{tr} denote the track widths of the front, middle, and rear axles, respectively.

3.6 Vertical dynamics

To accurately model the vertical dynamics, the evolution of pressure P_s in each air suspension is therefore crucial. Under the assumptions of constant temperature and linear volume variation with vertical displacement, the pressure dynamics are governed by the following nonlinear differential equation, derived earlier in (2.8):

$$\dot{P}_{s,i} = \frac{RT_s}{V_0 - z_i A_{\text{ef,i}}}\dot{m}_{s,i} - \frac{P_{si}A_{\text{ef,i}}}{V_0 - z_i A_{\text{ef,i}}}\dot{z}_i \tag{3.20}$$

where i denotes the 6 air suspensions, one for each wheel.

The vertical suspension forces $F_{zs,i}$ generated by the air springs are critical for maintaining vehicle stability, especially in roll-prone maneuvers. Each suspension corner generates a vertical force modelled as the air spring and damping forces:

$$F_{zs,i} = (P_{si} - P_{atm})A_{\text{ef},i} - \dot{z}_i D_{z,i} \tag{3.21}$$

where P_{si} is the pressure in the air spring, $A_{\text{ef},i}$ is the effective area of the air spring in m^2.

The vertical velocities $\dot{z}_i$ at each suspension corner are only modelled with the roll in consideration. When the vehicle rolls, the left and right sides of the chassis experience opposite vertical movements:

$$z_1 = \frac{w_{sf}}{2}\tan(\phi), \qquad \text{(front left)} \tag{3.22}$$
$$z_2 = -\frac{w_{sf}}{2}\tan(\phi), \qquad \text{(front right)} \tag{3.23}$$
$$z_3 = \frac{w_{sm}}{2}\tan(\phi), \qquad \text{(middle left)} \tag{3.24}$$
$$z_4 = -\frac{w_{sm}}{2}\tan(\phi), \qquad \text{(middle right)} \tag{3.25}$$
$$z_5 = \frac{w_{sr}}{2}\tan(\phi), \qquad \text{(rear left)} \tag{3.26}$$
$$z_6 = -\frac{w_{sr}}{2}\tan(\phi), \qquad \text{(rear right)} \tag{3.27}$$

and similarly the displacement velocity:

$$\dot{z}_1 = \frac{w_{sf}}{2}\dot{\phi}\cos(\phi), \qquad \text{(front left)} \tag{3.28}$$
$$\dot{z}_2 = -\frac{w_{sf}}{2}\dot{\phi}\cos(\phi), \qquad \text{(front right)} \tag{3.29}$$
$$\dot{z}_3 = \frac{w_{sm}}{2}\dot{\phi}\cos(\phi), \qquad \text{(mid left)} \tag{3.30}$$
$$\dot{z}_4 = -\frac{w_{sm}}{2}\dot{\phi}\cos(\phi), \qquad \text{(mid right)} \tag{3.31}$$
$$\dot{z}_5 = \frac{w_{sr}}{2}\dot{\phi}\cos(\phi), \qquad \text{(rear left)} \tag{3.32}$$
$$\dot{z}_6 = -\frac{w_{sr}}{2}\dot{\phi}\cos(\phi). \qquad \text{(rear right)} \tag{3.33}$$

To accurately capture the nonlinear behaviour of the tires, it is essential to compute the vertical tire loads at each wheel. During turning maneuvers, the vehicle body rolls, causing lateral load transfer, a shift of vertical force from the inner wheels to the outer wheels. The load transfer is modeled as an effect of the torque around the roll center, as in [15], modified to include the vertical suspension forces' induced torque. The weight transfer, ΔF_z is calculated as follows:

$$\Delta F_{z,f} = -\frac{D_{\phi,f}\dot{\phi}}{w_{tf}/2} - \frac{K_{\phi,f}\phi}{w_{tfs}/2} + \frac{w_{tf}}{2}\cdot\frac{F_{zs1} - F_{zs2}}{w_{sr}/2} \tag{3.34}$$
$$\Delta F_{z,m} = -\frac{D_{\phi,m}\dot{\phi}}{w_{tm}/2} - \frac{K_{\phi,m}\phi}{w_{tm}/2} + \frac{w_{tm}}{2}\cdot\frac{F_{zs3} - F_{zs4}}{w_{sm}/2} \tag{3.35}$$
$$\Delta F_{z,r} = -\frac{D_{\phi,r}\dot{\phi}}{w_{tr}/2} - \frac{K_{\phi,r}\phi}{w_{tr}/2} + \frac{w_{tr}}{2}\cdot\frac{F_{zs5} - F_{zs6}}{w_{sr}/2} \tag{3.36}$$

where $D_{\phi,(f,m,r)}$ is the roll damping coefficient for the front, middle, and rear axles, respectively. $K_{\phi,(f,m,r)}$ is the roll stiffness coefficient for the front, middle, and rear axle.

Finally, each tire load, F_{zi}, is computed as the sum of the static and dynamic load transfer, which accounts for the vertical force at each tire and the roll-induced

force, and is divided by the number of tires on each axle.

$$F_{z1} = \frac{m_{a1}g}{2} + \frac{\Delta F_{z,f}}{2} \tag{3.37}$$

$$F_{z2} = \frac{m_{a1}g}{2} - \frac{\Delta F_{z,f}}{2} \tag{3.38}$$

$$F_{z3} = \frac{m_{a2}g}{4} + \frac{\Delta F_{z,m}}{4} \tag{3.39}$$

$$F_{z4} = \frac{m_{a2}g}{4} - \frac{\Delta F_{z,m}}{4} \tag{3.40}$$

$$F_{z5} = \frac{m_{a3}g}{2} + \frac{\Delta F_{z,r}}{2} \tag{3.41}$$

$$F_{z6} = \frac{m_{a3}g}{2} - \frac{\Delta F_{z,r}}{2} \tag{3.42}$$

where $m_{a,(1,2,3)}$ denotes the portion of the vehicle's mass supported by the front, middle, and rear axles, respectively. With the vertical dynamics now defined, the complete nonlinear vehicle model $\dot{x} = f(x, u, \delta)$ with the inputs of the torque τ and mass flow rate $\dot{m}_{si}$ can be constructed and serves as foundation for the model-based control design. Parameter values for the vehicle dynamics model are listed in Table 3.2:

Parameter	**Unit**	**Value**
A_f	m^2	Confidential
A_{ef}	m^2	Confidential
C_d	Unitless	0.7
C_r	Unitless	0.008
D_ϕ, D_{ϕ_f,ϕ_m,ϕ_r}	$N \cdot m \cdot s/\text{rad}$	Confidential
D_z, D_{z_f,z_m,z_r}	$N \cdot s/\text{m}$	Confidential
g	m/s^2	9.81
h_{roll}	m	Confidential
I_{xx}	$kg \cdot m^2$	Confidential
I_{yy}	$kg \cdot m^2$	Confidential
I_{zz}	$kg \cdot m^2$	Confidential
K_ϕ, K_{ϕ_f,ϕ_m,ϕ_r}	$N \cdot m/\text{rad}$	Confidential
l_f, l_m, l_r	m	Confidential
m	kg	Confidential
ma	kg	(Confidential)
η	Unitless	1
r	m	Confidential
ρ_{air}	kg/m^3	1.225
w_{sf}, w_{sm}, w_{sr}	m	Confidential
w_{tf}, w_{tm}, w_{tr}	m	Confidential

Table 3.2: Key vehicle and environmental parameters used in the dynamics model.

4

Control System Design

The feedback control system consists of four main components: the plant, the sensor, the controller, and the actuator. The plant is the system that we want to control, in this case, a 6x2 truck. The sensors measure the output of the plant, including positions, angles, and velocities. The controller computes the control input based on the measured output and the desired setpoint. Finally, the actuator applies the control input to the plant, thereby changing its behavior [16]. Traditional control methods, such as PID controllers, rely on simple control laws based on present error. In contrast, MPC excels at handling setpoint changes and enforcing constraints, [17]. MPC is a controller that is particularly suitable for complex multivariable systems with constraints, [18]. At each sampling instant k, the controller predicts future system behaviour over a prediction horizon using a model of the system, computes the optimal sequence of control inputs given a certain reference, and applies only the first input before repeating the process at the next time step.

4.1 Nonlinear Model Predictive Control

In this thesis, a Nonlinear Model Predictive Control (NMPC) approach is implemented to address the system's inherent nonlinearities, including roll dynamics, air suspension pressure behaviour, and nonlinear tire forces.

The primary objective of the proposed NMPC controller is to enhance roll stability and maintain the desired speed of a heavy vehicle equipped with active air suspension, while ensuring compliance with physical and operational constraints. NMPC is particularly well-suited for this application. It can explicitly account for nonlinear dynamics, input and state constraints, and anticipated disturbances, such as future steering maneuvers by directly incorporating them into the optimization problem formulation [19].

At each control update step, the NMPC controller solves an optimization problem over a finite prediction horizon. The problem is defined as follows through the following constrained optimization problem:

$$
\begin{aligned}
\min_{u_k} \quad & \sum_{k=0}^{N-1} (x_k - x_{\text{ref}})^T Q (x_k - x_{\text{ref}}) + u_k^T R u_k \\
\text{subject to} \quad & x_{k+1} = f_d(x_k, u_k, \delta), \quad k = 0, \ldots, N-1 \\
& x_0 = x(t) \\
& u_1 \in [-10{,}000,\ 10{,}000] \\
& u_{2:7} \in [-1,\ 1] \\
& x_k \in \mathcal{X}, \quad u_k \in \mathcal{U}
\end{aligned}
\tag{4.1}
$$

where x_k denotes the predicted state vector at time step k, and u_k the control input vector. The cost function penalizes deviations from a reference trajectory x_{ref} using the state weighting matrix Q, and control effort using the control weighting matrix R. The control input $u \in \mathbb{R}^7$ includes the motor torque u_1 and six valve signals $u_{2:7}$ regulating air mass flow in the suspension bellows. The state vector x consists of longitudinal and lateral velocity, yaw angle and yaw rate, roll angle and roll rate, and the internal pressures of each air spring, as presented earlier and found in Table 3.1. The discrete-time dynamics function $f_d(x_k, u_k, \delta)$ defines how the state evolves over time and is obtained by discretizing the continuous nonlinear vehicle dynamics using a fourth-order Runge-Kutta (RK4) method. RK4 is commonly used for discretizing nonlinear dynamical systems due to its balance between accuracy and computational efficiency [20].

Physical feasibility is ensured through hard constraints on the inputs. The motor torque is limited by

$$-10000 \leq u_1 \leq 10000$$

where u_1 is the torque in [Nm] and the suspension valve inputs are bounded by:

$$-1 \leq u_{2:7} \leq 1$$

where $u_{2:7}$ are unitless and positive values represent increasing pressure, and negative values represent decreasing pressure. This formulation allows the NMPC to maintain performance and safety by ensuring that the truck operates within feasible bounds while pre-emptively counteracting roll-inducing maneuvers using predictive knowledge of the trajectory.

4.1.1 Solver Strategy and Numerical Methods

The multi-shooting method was chosen for the controller implementation, as it provides greater numerical stability and flexibility in handling nonlinear dynamics [21]. While single shooting only optimizes the control inputs and integrates the state trajectory forward from the initial condition, multiple shooting treats both the states and inputs as decision variables and enforces continuity constraints across the prediction horizon. This structure is more robust to poor initial guesses and better suited for systems with nonlinearities and constraints. The primary drawback of multiple shooting is the increased number of decision variables and constraints, which results in a larger and computationally more demanding optimization problem.

Solving the nonlinear optimization problem with MPC requires an efficient and reliable solver. In this work, FATROP was deemed the best fit. While other solvers are compatible with CasADI, their characteristics and performance vary significantly. FATROP is a nonlinear programming (NLP) solver developed for real-time applications. It is particularly well-suited for embedded control tasks, such as MPC. FATROP is integrated with the CasADi framework and uses automatic differentiation and sparsity-exploiting linear algebra to accelerate computation [22].

To reduce computation time, a critical factor throughout this work due to the nonlinear and stiff dynamics, warm-starting has been applied in the NMPC formulation. Warm-starting is a technique where the solution from a previous iteration is used as the initial guess for the next iteration, thereby accelerating convergence. Since the optimization problem is solved repeatedly every 100 ms with only minor variations in the initial state and disturbance trajectory, the solution from the previous iteration serves as an effective initial guess for subsequent iterations. This technique is particularly valuable for non-convex problems, where solver performance is sensitive to initialization, and convergence time depends heavily on the initial guess for the state and input trajectories, [23]. By warm-starting both the predicted state trajectory and control inputs, convergence speed and reliability are improved significantly.

4.1.2 Parameter Tuning

When tuning an NMPC, it is crucial to balance control performance with computational feasibility and a reasonable computation time. A system with many states and control inputs often exhibits stiff dynamics, meaning it includes both fast and slow dynamics, [24], where tire forces are fast and suspension dynamics and roll motion are slow. Capturing both time scales accurately requires a short integration time step, which increases computational demands during the optimization process.

The choice of weight matrices Q and R in the NMPC cost function determines control performance and stability. The state weighting matrix Q determines how strongly the controller penalizes deviations from the reference trajectory, while the control weighting matrix R penalizes the control effort [18].

In this work, the Q matrix is designed to prioritize tracking of the longitudinal velocity v_x and roll angle ϕ, as these are key indicators of performance and stability:

$$\mathbf{Q} = \begin{bmatrix} 10000 & 0 & 0 & 0 & 0 & 0 & 0 & 0 & 0 & 0 & 0 & 0 \\ 0 & 0 & 0 & 0 & 0 & 0 & 0 & 0 & 0 & 0 & 0 & 0 \\ 0 & 0 & 0 & 0 & 0 & 0 & 0 & 0 & 0 & 0 & 0 & 0 \\ 0 & 0 & 0 & 0 & 0 & 0 & 0 & 0 & 0 & 0 & 0 & 0 \\ 0 & 0 & 0 & 0 & 100000 & 0 & 0 & 0 & 0 & 0 & 0 & 0 \\ 0 & 0 & 0 & 0 & 0 & 0 & 0 & 0 & 0 & 0 & 0 & 0 \\ 0 & 0 & 0 & 0 & 0 & 0 & 0 & 0 & 0 & 0 & 0 & 0 \\ 0 & 0 & 0 & 0 & 0 & 0 & 0 & 0 & 0 & 0 & 0 & 0 \\ 0 & 0 & 0 & 0 & 0 & 0 & 0 & 0 & 0 & 0 & 0 & 0 \\ 0 & 0 & 0 & 0 & 0 & 0 & 0 & 0 & 0 & 0 & 0 & 0 \\ 0 & 0 & 0 & 0 & 0 & 0 & 0 & 0 & 0 & 0 & 0 & 0 \\ 0 & 0 & 0 & 0 & 0 & 0 & 0 & 0 & 0 & 0 & 0 & 0 \end{bmatrix}$$

Other states are assigned zero weights since they are not the primary focus of the control objective. This design choice ensures that the suspension system is responsible for maintaining roll stability, rather than relying on speed reduction, which, while effective, would reduce the intended evaluation of active suspension performance.

The control weighting matrix R was chosen to impose minimal penalty on the air suspension valves, effectively allowing the NMPC to exploit their full authority without restriction.

$$\mathbf{R} = \begin{bmatrix} 10 & 0 & 0 & 0 & 0 & 0 & 0 \\ 0 & 0.01 & 0 & 0 & 0 & 0 & 0 \\ 0 & 0 & 0.01 & 0 & 0 & 0 & 0 \\ 0 & 0 & 0 & 0.01 & 0 & 0 & 0 \\ 0 & 0 & 0 & 0 & 0.01 & 0 & 0 \\ 0 & 0 & 0 & 0 & 0 & 0.01 & 0 \\ 0 & 0 & 0 & 0 & 0 & 0 & 0.01 \end{bmatrix}$$

This design choice encourages active suspension engagement for roll stabilization. Both Q and R were tuned through simulations to balance reference tracking, rollover prevention, and computational efficiency. A high value in R leads to smoother inputs but less responsive behaviour, while a low value improves tracking at the cost of actuation effort.

The prediction horizon length and time discretization are critical design parameters in NMPC, as they directly affect both the control performance and computational time. In this implementation, a prediction horizon of 5 seconds was selected, discretized into $N = 100$ intervals with a step size of $\Delta t = 0.05$ seconds. This resolution ensures that the controller can accurately capture the vehicle's fast dynamics while predicting far enough into the future to anticipate critical manoeuvres such as lane changes or cornering.

To balance accuracy with computational efficiency, the controller is designed with two different sampling rates using Zero-Order Hold (ZOH). The optimal control se-

quence is applied to the system and held constant until the next control update. This approach ensures that the plant receives a continuous control signal despite the discrete-time optimization and reduces the need for recomputation within the control interval. In this implementation, the control input is updated every 0.1 seconds and held constant over that interval using ZOH, while the internal prediction dynamics operate at a finer resolution of 0.05 seconds.

4.1.3 Integration in Simulink

The NMPC controller was integrated into the Simulink environment using a MATLAB Systems block. This block has an interactive interface between Simulink's signal-based framework and the object-oriented NMPC controller implemented in MATLAB. The structure of the NMPC feedback loop used in this work is shown in Figure 4.1, the controller receives a reference trajectory and measured state vector from the VTM plant, computes an optimal control input sequence by solving a model-based optimal control problem, and applies only the first control input u_{opt} at each update step. An additional predicted lateral velocity v_y is included as an open-loop input in the NMPC formulation because directly observing or estimating v_y was challenging. Including it in this way improved the prediction accuracy of other states in the model. Furthermore, all states used in the controller are assumed to be directly measurable from the VTM model, and therefore no dedicated observer has been implemented or described in the report.

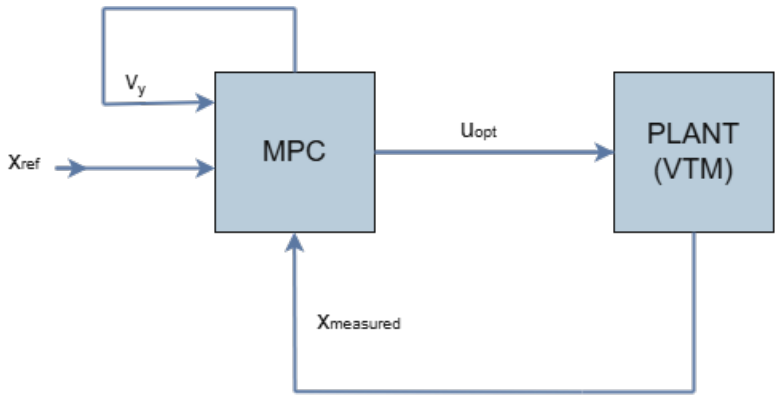

Figure 4.1: Block diagram of the closed-loop NMPC implementation

4.2 Baseline Controller

To evaluate the performance of the developed NMPC strategy, a baseline controller was developed and implemented for comparison. The baseline consists of a simple Proportional-Integral (PI) controller designed to control the vehicle's longitudinal velocity. This controller tracks a constant reference velocity in closed-loop operation, [25]:

$$
\begin{aligned}
e(t) &= v_{x,\text{ref}} - v_x(t) \\
u(t) &= \text{sat}\left(K_p \cdot e(t) + K_i \int_0^t e(\tau)\, d\tau\right) \\
T(t) &= u(t) \cdot 10^4
\end{aligned}
\tag{4.2}
$$

where $e(t)$ denotes the longitudinal velocity tracking error, where $v_{x,\text{ref}}$ is the reference velocity and $v_x(t)$ is the current longitudinal velocity. The control input $u(t)$ is computed using proportional and integral gains, with $K_p = 2$ and $K_i = 1$. The saturation function $\text{sat}(\cdot)$ limits the control signal to the range $[-1, 1]$, representing actuator constraints. The resulting control input is scaled by a factor of 10^4 to obtain the torque $T(t)$, ensuring that the torque command falls within the same bounds as those used in the NMPC controller, i.e., $[-10000, 100000]$. To prevent errors in the integration of a saturated PI controller, an anti-windup strategy called clamping is used [26]. Steering control is applied as an open-loop input and is determined before simulation. The controller block diagram is illustrated in Figure 4.2.

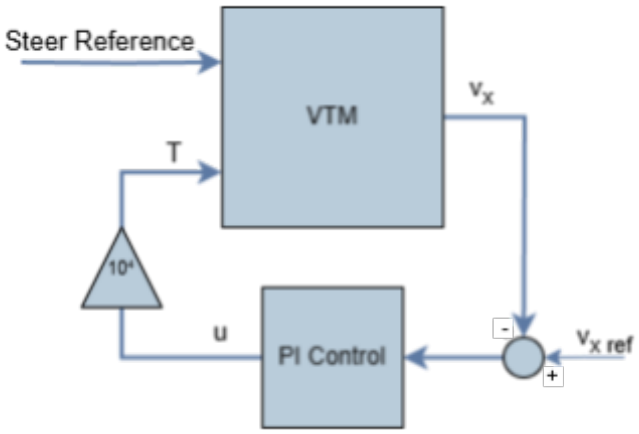

Figure 4.2: Baseline controller: PI controller block diagram

Furthermore, the baseline controller will have no control authority over the air suspension valves below, and the suspension will remain fully passive.

5
Simulation Results

In this chapter, the developed NMPC and baseline controller discussed in Chapter 4 are evaluated. They are simulated in Simulink using the extended air suspension VTM model derived in Chapter 2 with an Euler solver using a constant time step of 1 ms. The controller performance comparison is conducted across various driving and payload scenarios, with metrics evaluated in terms of performance and handling.

5.1 Evaluation Metrics

To compare the two controllers, the NMPC and the PI controller, several relevant metrics are defined and motivated in this section.

5.1.1 Lateral Load Transfer Ratio

To evaluate the risk of rollover, a commonly used metric is the lateral load transfer ratio, [27]. When a vehicle initiates a turn, it experiences lateral acceleration, which induces a roll and transfer of load from the inner wheels to the outer wheels. This results in an imbalance in vertical forces, where the outer wheels experience greater vertical force, $F_{z,\text{outer}}$ than the inner wheels, $F_{z,\text{inner}}$, i.e., $F_{z,\text{outer}} > F_{z,\text{inner}}$. If the lateral acceleration becomes too large, the vehicle exceeds a critical roll angle, ϕ_{crit}, at which the inner wheels will lose contact with the ground ($F_{z,\text{inner}} = 0$), indicating that a rollover has occurred. A common way to quantify the risk of rollover is through the Lateral Load Transfer Ratio (LTR), which normalizes the lateral load transfer with respect to the total vertical load on both sides [27]:

$$\Delta \bar{F}_z = \frac{F_{z,left} - F_{z,\text{right}}}{F_{z,\text{left}} + F_{z,\text{right}}} \tag{5.1}$$

where $F_{z,\text{left}}$ and $F_{z,\text{right}}$ represent the vertical forces on the left and right wheels, respectively. These can refer either to the total forces on the left and right sides of the vehicle or to the forces on each axle. Thus, a sufficient and necessary condition for a rollover to occur is $\Delta \bar{F}_z = \pm 1$.

5.1.2 Understeer Gradient

Another critical aspect of evaluating a vehicle's dynamics is its response to steering input. A key metric used for this purpose is the understeer gradient, which helps characterize whether a vehicle tends to understeer or oversteer.

Understeer occurs when the front tires are unable to generate sufficient lateral force for a given steering input, resulting in the vehicle turning less than intended. Conversely, oversteer refers to the condition where the rear tires lose grip, causing the vehicle to turn more than expected for the same steering input.

The understeer gradient K_{us} quantifies this behaviour during steady-state cornering. A positive gradient ($K_{us} > 0$) indicates understeer, a zero gradient ($K_{us} = 0$) corresponds to neutral steer, and a negative gradient ($K_{us} < 0$) signifies oversteer [28]. The understeer gradient can be calculated using the following formula derived in [29]:

$$K_{us} = \frac{1}{v_x}\left(\frac{\delta}{\omega_z} - \frac{L}{v_x}\right) \tag{5.2}$$

where v_x is the longitudinal velocity, δ is the average steering angle of the left and right front wheels, ω_z is the yaw rate, and L is the wheelbase of the vehicle. In the case of a 3-axle truck, the effective wheelbase L is computed as the average distance from the front axle to the middle and rear axles.

5.1.3 Roll, Pitch and Longitudinal Velocity

The performance of the controllers will also be evaluated using roll angle, longitudinal velocity, and pitch angle. Roll angle is a critical metric due to its direct relationship with rollover risk, especially the rearmost COG roll angle will be studied, as this section of the vehicle is typically the first to experience rollovers. During cornering, especially at higher speeds or with sudden steering inputs, a truck experiences lateral acceleration that induces roll. If this roll exceeds the critical threshold, denoted as ϕ_{crit}, the vehicle may enter a non-recoverable rollover state [27]. Hence, assessing the roll behaviour of the controllers is essential for ensuring safety. Additionally, roll angle plays a significant role in ride comfort. As demonstrated in [30], applying a reverse roll strategy, where the vehicle leans into the direction of a turn in anticipation, can reduce lateral forces acting on the driver and passengers. This results in a smoother and more comfortable experience.

Longitudinal velocity is another key performance indicator, as one of the primary controllable states in the developed controllers. Maintaining appropriate longitudinal velocity is relevant as it is one of the main objectives of the controllers.

Although pitch angle is not controlled by the controllers in this thesis, its behaviour is still relevant. Pitch motion affects the distribution of vertical loads across the axles, which in turn influences traction and handling. Ignoring pitch dynamics may lead to unintended behaviour. Therefore, studying pitch response provides insights into secondary effects of the control design and identifies areas for potential improvement.

5.2 Simulation Results and Discussion

This section defines the driving scenarios and compares the relevant performance metrics for each scenario. Note that the plotted simulation results begin after the actual simulation start time, allowing the system to reach a near steady-state condition. The full inputs and state trajectory predictions of the NMPC can be found in Appendix A.

5.2.1 Constant Turn

Scenario Description

The first scenario involves the vehicle travelling at a constant speed of 43.2 km/h equivalent to 12 m/s. This moderate speed is chosen to analyze the behavior of the truck without causing rollover, allowing safe evaluation of the controller during a constant turn. After 4 seconds, a step input is applied to the steering reference to simulate a quick left turn. The scenario is designed to evaluate the controller's steady-state performance under a constant, non-zero steering input, with a specific focus on the understeer gradient and lateral load transfer metrics.
The steering reference signal, denoted as $\delta_{\text{ref}}(t)$, is defined as:

$$\delta_{\text{ref}}(t) = \begin{cases} 0, & \text{for } t < 4 \\ 8.59, & \text{for } t \geq 4 \end{cases} \tag{5.3}$$

where δ_{ref} is the reference steering angle provided to VTM, expressed in degrees. The scenario is simulated under two loading conditions: first, with a 5-ton payload, and second, with an 18.17-ton payload, which corresponds to the maximum legal weight for a heavy truck on Swedish roads [31]. The steering reference is shown in Figure 5.1.

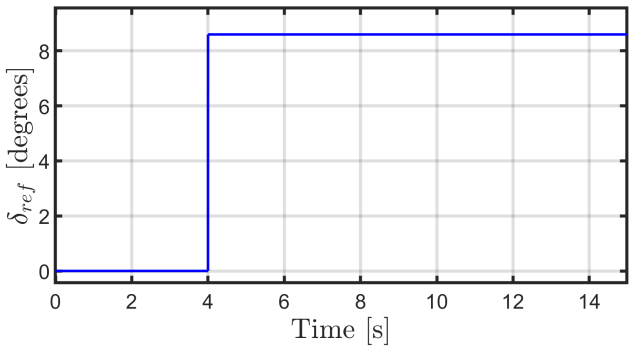

Figure 5.1: Constant turn steering reference signal

Results and Discussion

Figure 5.2 presents the roll angle responses for both scenarios. For the passive system, it can be noted that when the turn starts, the roll angle exhibits a sharp increase, followed by a steady-state behavior. In contrast, the NMPC controller,

with access to the steering reference and a 5-second prediction horizon, utilizes the suspension via valve control to lean into the turn, thereby reducing the peak roll. The strategy is necessary due to the slow dynamics of the air suspension system, see Appendix A for NMPC control signals and predicted trajectories. The result is a reduction in peak roll angle of approximately 45% for a 5 ton payload and 21% for the fully loaded 18.17 ton truck. This indicates a lower roll over risk and more comfortable ride for the driver.

While the passive suspension system maintains a constant roll angle after the peak, the NMPC continues to reduce it gradually as the suspension builds additional counteracting force. As expected, the weight of the payload has a significant impact on roll, and it is evident that the suspension has more control authority with a lower payload.

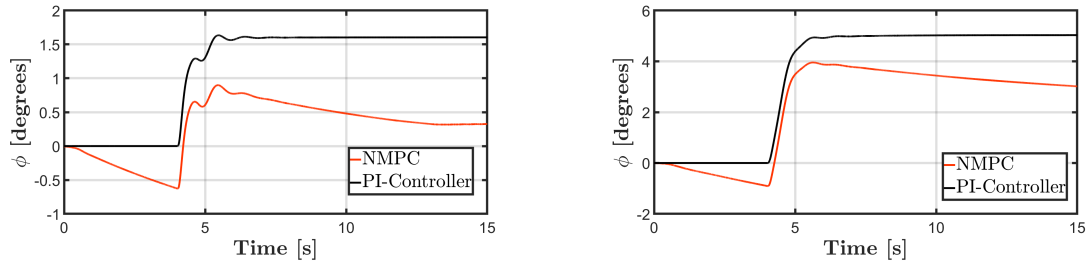

(a) 5 ton payload **(b)** Full 18.17 ton payload

Figure 5.2: Comparison of roll angle for a constant turn and different payloads

In Figure 5.3, the longitudinal velocity is presented. Consistently, for both payloads, the PI controller maintains the velocity close to the reference until the turn initiates, where the speed dips slightly, causing a slight overshoot of the reference thereafter. However, the NMPC predicts the turn and preemptively increases the velocity just before the turn starts to maintain the reference velocity.

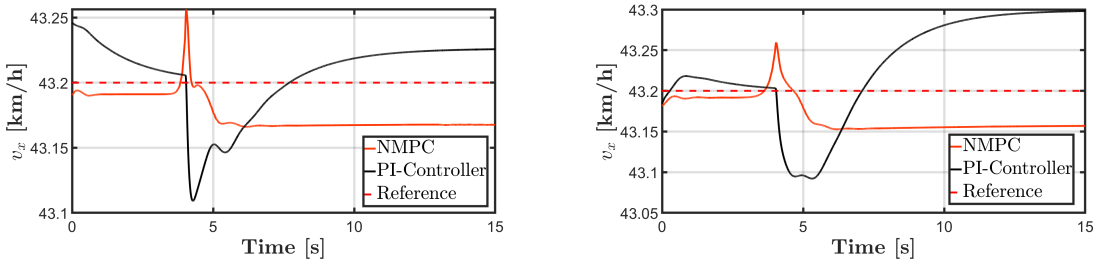

(a) 5 ton payload **(b)** Full 18.17 ton payload

Figure 5.3: Comparison of longitudinal velocity for a constant turn and different payloads

Figure 5.4 illustrates the LTR for each axle during the constant turn. The passive suspension system exhibits a high peak in LTR that then remains steady. However, for the NMPC, the two rearmost axles' LTR values are increased in anticipation of

the turn induced by the pre-emptive roll, and the negative peaks are reduced and continuously improved as the roll decreases. Although the LTR value for the front axle increases with NMPC, this does not indicate an increased rollover risk, as the rear axles, which initiate rollovers, are better controlled.

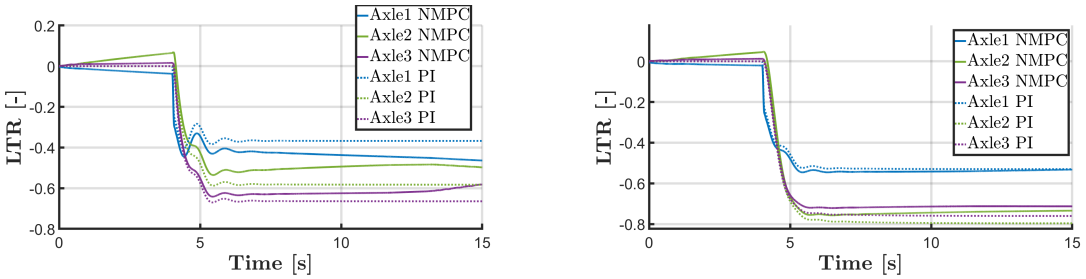

(a) 5 ton payload **(b)** Full 18.17 ton payload

Figure 5.4: Comparison of lateral load transfer ratio for a constant turn and different payloads

Figure 5.5 shows the understeer gradient during the steady-state interval $t = [6, 15]$. For the 5-ton payload, the PI controller yields a positive steady-state gradient, indicating mild understeer. The NMPC further increases this gradient, resulting in a more pronounced understeer condition. Although the handling characteristics worsen with the 5-ton payload, the change is negligible for a fully loaded 18.17 ton truck. In that case, both controllers maintain the gradient near zero, corresponding to neutral steer behaviour. However, it is noted that both scenarios indicate an increase in understeering, which is undesirable for handling.

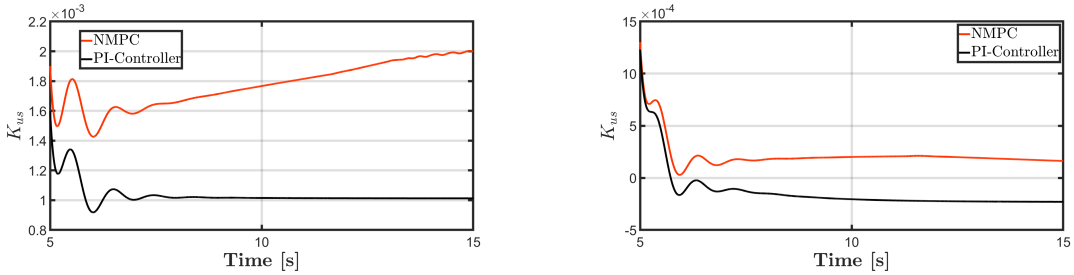

(a) 5 ton Payload **(b)** Full 18.17 ton payload

Figure 5.5: Comparison of Understeer Gradient for a Constant Turn and different payloads

Figure 5.6 presents the pitch angles for both scenarios. Pitch behavior influences the overall handling characteristics of the vehicle and, in this case, an increase in pitch angle is observed as the vehicle leans into the corner. This upward trend may contribute to degraded handling.

The increase in pitch is a result of the suspension dynamics during cornering. As the NMPC controller actuates the suspension by reducing pressure on the left side and increasing it on the right, the distribution of vertical forces between the front

and rear axles is altered. This imbalance causes the vehicle to pitch forward. The effect is more pronounced due to the configuration of the suspension system, where two air suspension units are mounted at the rear, leading to a differential response compared to the front. The forward pitch can potentially shift the load distribution unfavorably, thereby affecting the steering response, due to changes in vertical forces on the tires. And since the NMPC does not consider pitch dynamics, this might lead to unfavourable handling performances.

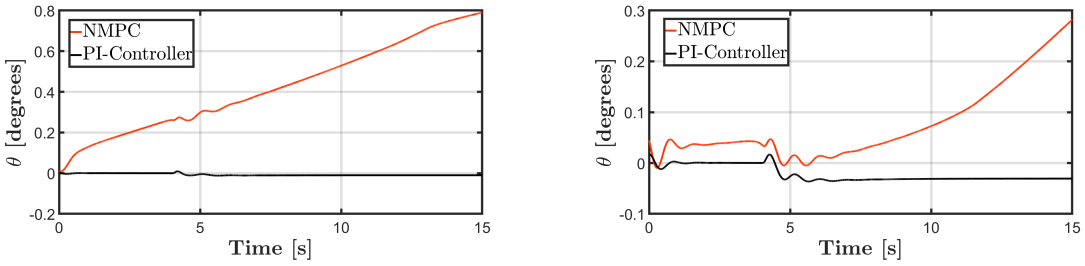

(a) 5 ton Payload **(b)** Full 18.17 ton payload

Figure 5.6: Comparison of Pitch for a Constant Turn and different payloads

Summary and comparison of the values presented can be seen in Table 5.2

Table 5.1: Metric comparison during the constant turn scenario

Metric	Controller	5 Ton	Full
Peak Roll Angle [Degrees]	NMPC	0.8991	3.9554
	PI	1.6349	5.0390
Improvement [%]		45%	21%
Peak LTR (All axles)	NMPC	-0.6418	-0.7571
	PI	-0.6701	-0.7966
Improvement [%]		4.22%	4.96%
Mean LTR, Axle 1, $t \in [8, 15]$s	NMPC	-0.4444	-0.5392
	PI	-0.3675	-0.5297
Improvement [%]		-20.93%	-1.79%
Mean LTR, Axle 2, $t \in [8, 15]$s	NMPC	-0.4915	-0.7410
	PI	-0.5826	-0.7955
Improvement [%]		15.64%	6.85%
Mean LTR, Axle 3, $t \in [8, 15]$s	NMPC	-0.6168	-0.7136
	PI	-0.6642	-0.7595
Improvement [%]		7.14%	6.04%
Mean USG, $t \in [8, 15]$s	NMPC	0.0018	0.0002
	PI	0.0010	-0.0002

5.2.2 Ramp-Hold Turn

Scenario Description

The second scenario evaluates the controller's performance during a dynamic maneuver in which the steering angle gradually increases over time before stabilizing. This scenario emulates a smooth entry into a long corner. The scenario is particularly useful for detecting rollover characteristics under more realistic driver inputs. The vehicle is running at a constant velocity of the maximum legal speed for a heavy truck in Sweden, 90km/h, [31].
4 seconds into the scenario, a ramp input begins with a slope of 0.573°/s, continuing linearly for 5 seconds until reaching a final value of 2.86°, which is then held constant for the remainder of the simulation. This shape approximates a gradual steering input, as might be observed in driver behavior during corner entry, followed by a steady hold throughout the turn. The steering reference signal, denoted as $\delta_{\text{ref}}(t)$, is defined as:

$$\delta_{\text{ref}}(t) = \begin{cases} 0, & \text{for } t < 4 \\ 0.573(t-4), & \text{for } 4 \leq t < 9 \\ 2.86, & \text{for } t \geq 9 \end{cases} \tag{5.4}$$

where δ_{ref} is the reference steering angle provided to VTM, expressed in degrees. As with the previous case, this scenario is tested under both 5-ton and full 18.17 ton payload conditions. The corresponding steering reference signal is illustrated in Figure 5.7.

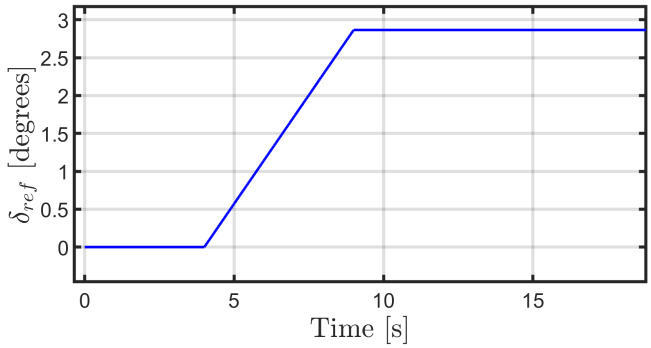

Figure 5.7: Ramp-Hold Turn, Steering Reference Signal

Results and Discussion

In Figure 5.8, the roll angle is shown for the Ramp-hold steering input. The NMPC outperforms the PI controller. Though a combination of leaning into the turn and continuous counteraction forces from the suspension counteract the roll. For a 5 ton payload the peak roll angle gets improved by 33.45%, and for the fully loaded 18.17 ton truck, the PI controller rolls over, as can be seen by the sharp increase in roll angle at approximately 15 seconds after reaching a critical roll angle, ϕ_{crit}. In contrast, the NMPC avoids the rollover and has a consistently lower roll angle throughout the maneuver.

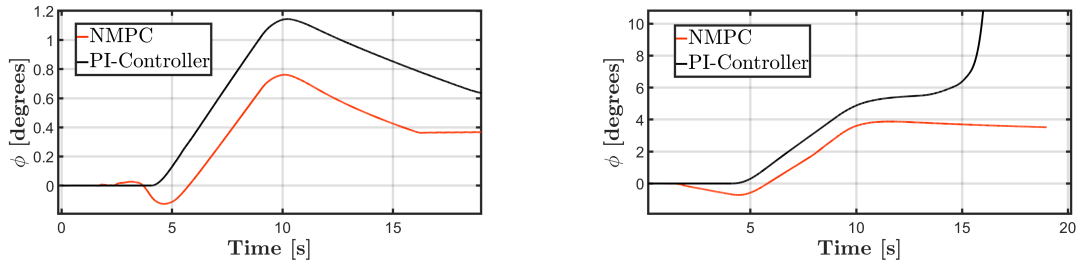

(a) 5 Ton Payload **(b)** Full 18.17 ton payload

Figure 5.8: Comparison of roll angle for ramp-hold steering and different payloads

In Figure 5.9, the longitudinal velocity is seen to track the velocity well for both scenarios until the rollover occurs for the PI controller with a full 18.17-ton payload, as the wheels lose contact with the ground. This indicates that utilizing the active air suspension prevents the vehicle from rolling over.

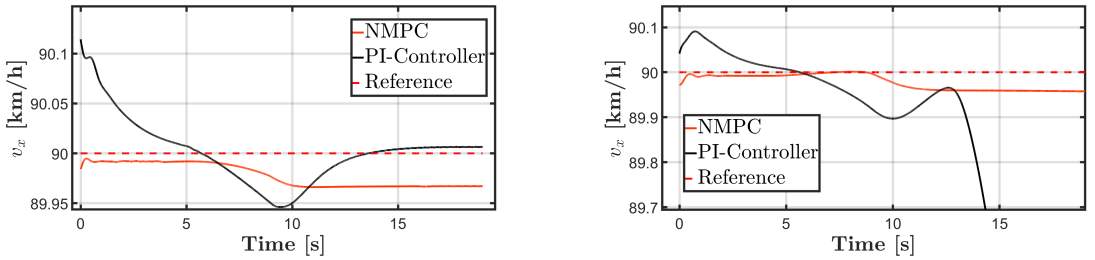

(a) 5 ton payload **(b)** Full 18.17 ton payload

Figure 5.9: Comparison of longitudinal velocity for ramp-hold steering and different payloads

As seen in Figure 5.10, the Lateral Transfer Ratio (LTR) for each axle is plotted. The results show an improvement in the peak LTR values of the rear axles, which are the most critical with respect to rollover prevention. While the front axle LTR is increased, this has limited impact on rollover risk, as the front axle is the least likely to experience wheel lift, given that its LTR remains below 0.5 in magnitude. This behaviour is further illustrated in the case where a rollover occurs under the PI controller with a fully loaded 18.17 ton truck. It is observed that the second axle loses ground contact first (LTR = -1), indicating that all the normal force has shifted to the right tire, followed by the rear axle, and finally the front axle. This progression highlights that a controller-induced increase in front axle LTR does not significantly raise the risk of rollover, provided that it reduces the LTR on the more rollover-prone rear axles.

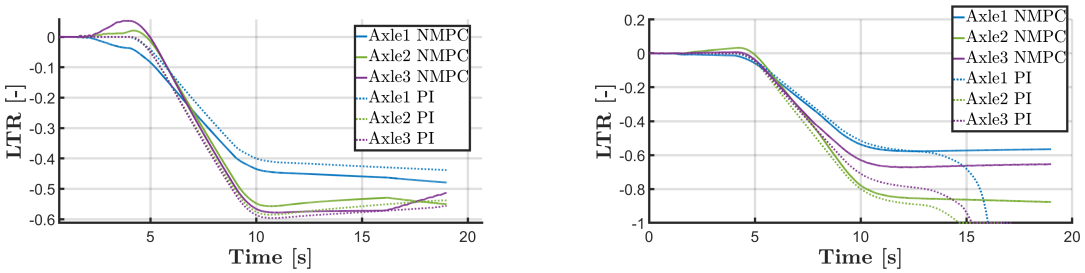

(a) 5 Ton Payload

(b) Full 18.17 ton payload

Figure 5.10: Comparison of lateral Load transfer ratio for ramp-hold steering and different payloads

The simulation results highlight the strengths of the NMPC system with active suspension, demonstrating its ability to prevent rollover during a realistic, rollover-prone maneuver. This showcases the safety benefits provided by the NMPC approach. It also indicates that driver comfort is improved for the NMPC, as the peak roll angle is decreased while maintaining the same constant velocity as the baseline PI controller.
Summary and comparison of the values presented can be seen in Table 5.2, and the pitch response can be found in Appendix B.

Table 5.2: Metric Comparison: Ramp-hold Turn

Metric	Controller	5 Ton	Full
Peak Roll Angle [Degrees]	NMPC	0.7614	3.8741
	PI	1.1441	Rollover
Improvement [%]		33.45%	N/A
Peak LTR (All axles)	NMPC	-0.5782	-0.8770
	PI	-0.5967	-1.0000
Improvement [%]		3.10%	12.30%

5.2.3 Lane Change

Scenario Description

The third scenario is designed to emulate a single lane-change maneuver at a speed of 80km/h. To achieve this, a single cycle of a sinusoidal steering input is applied after 4 seconds, defined as:

$$\delta_{ref}(t) = \begin{cases} A\sin(2\pi f t), & \text{for } 4 < t < 7.22 \\ 0, & \text{otherwise} \end{cases} \tag{5.5}$$

where $\delta_{ref}(t)$ represents the reference steering angle in degrees. The amplitude, $A = 1.72$ degrees, determines the maximum steering angle, and the frequency, $f = 0.31$ Hz, defines the duration of the sinusoidal cycle. These parameters are selected to approximate the steering reference of a single lane-change maneuver.

The steering reference is shown in Figure 5.11. This scenario is chosen to investigate the controller's performance during rapid steering maneuvers by the driver.

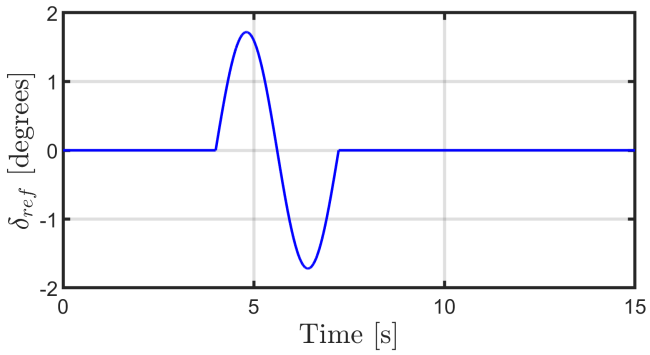

Figure 5.11: Lane change, Steering Reference Signal

Results and Discussion

As shown in Figure 5.12, the roll angle response for the lane change scenario demonstrates that the NMPC leans into the initial left turn. However, this leaning is less pronounced compared to the constant turn, likely to preserve the ability to recover for the subsequent right turn. The NMPC does not improve the first roll angle peak but achieves a reduction in the second. Specifically, the first peak worsens by 0.53% and 6.88% , while the second peak improves by 23.88% and 8.78%. This behavior is likely a result of the air suspension system's slow dynamics, which are unable to respond quickly enough during a rapid maneuver.

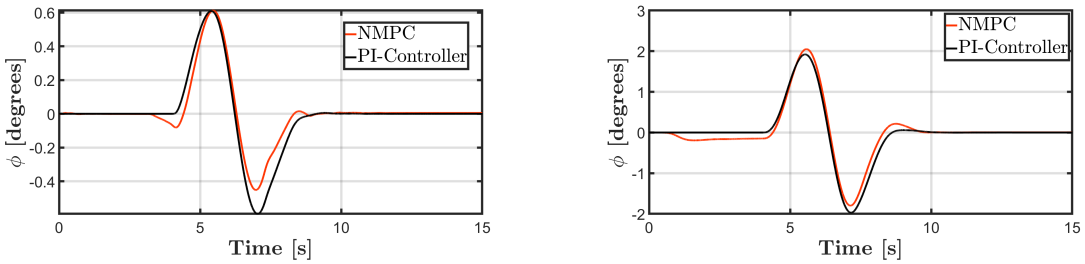

(a) 5 ton payload **(b)** Full 18.17 ton payload

Figure 5.12: Comparison of Roll angle for a lane change and different payloads

As seen in Figure 5.13, both controllers can follow the reference closely, as this maneuver does not cause significant deceleration.

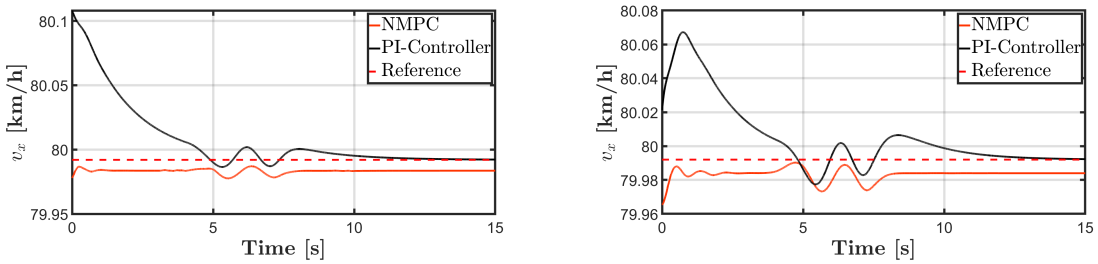

(a) 5 Ton Payload **(b)** Full 18.17 ton payload

Figure 5.13: Comparison of Longitudinal Velocity for a lane change and different payloads

The Load Transfer Ratio (LTR) for the lane change maneuver, shown in Figure 5.14, is noteworthy as both scenarios exhibit slightly higher LTR peaks, even in the second roll angle peak, which was reduced. Specifically, with 5 ton payload, the LTR increases by 3.34% and 3.22% , while with a full 18.17 ton payload, it increases by 1.84% and 2.25%.

However, since the maneuver does not approach a rollover condition with the LTR remaining below 0.3, these increases can be considered acceptable, particularly as a lower second roll peak accompanies them.

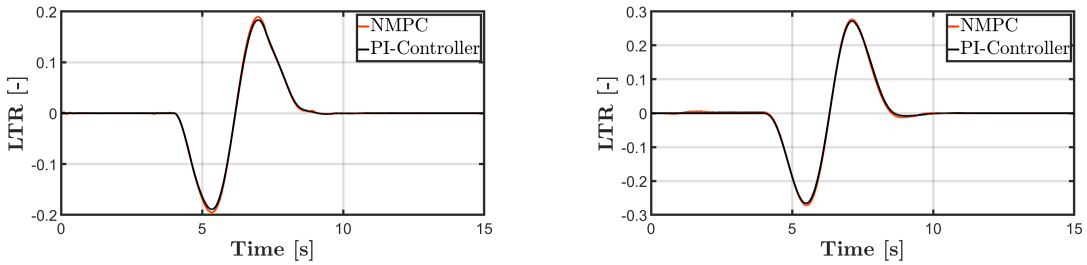

(a) 5 Ton Payload **(b)** Full 18.17 ton payload

Figure 5.14: Comparison of Lateral Load Transfer Ratio for a lane change and different payloads

This scenario highlights the weaknesses of the NMPC system. Even though the system successfully suppresses the second roll angle peak, the LTR does worsen slightly as the slow dynamics of the air suspension cannot adapt to the fast left-to-right turn during the lane change.

Summary and comparison of the values presented can be seen in Table 5.3, and the pitch response can be found in Appendix B.

Table 5.3: Metric Comparison: Lane Change

Metric	Controller	5 Ton	Full
Max Roll Angle [Degrees]	NMPC	0.6126	2.0513
	PI	0.6094	1.9213
Improvement [%]		-0.53%	-6.77%
Min Roll Angle [Degrees]	NMPC	-0.4517	-1.7977
	PI	-0.5934	-1.9708
Improvement [%]		23.88%	8.78%
Max Overall LTR	NMPC	0.1895	0.2768
	PI	0.1834	0.2718
Improvement [%]		-3.34%	-1.84%
Min Overall LTR	NMPC	-0.1952	-0.2721
	PI	-0.1892	-0.2661
Improvement [%]		-3.22%	-2.25%

5.2.4 Comparison of Controller Performance across Scenarios

The scenarios highlight the strengths and limitations of the air suspension NMPC system. The constant turn highlighted improved peak and steady-state LTR values, reducing the rollover risks and significantly lower roll angles, indicating a more comfortable ride. However, it also showcased a slight increase in understeering characteristics, indicating worse handling performance, which is likely attributed to the forward pitch changing the distribution of normal forces.

The Ramp-hold steer scenario showcases the main strength of the controller, which is avoiding rollover, a significant safety improvement. Through both a reduction in the LTR index of rollover prone axles and a decrease in peak roll angles. This shows the controller is superior to the passive suspension PI controller in a realistic rollover prone scenario.

The lane change scenario highlights the limitations of the air suspension system when subjected to rapid alternating steering inputs, as the change in force from the suspension is slow due to the air suspension bellows filling or draining of air. However, the controller still improved the secondary roll angle peak, which may have slightly improved ride comfort.

6
Concluding Remarks

6.1 Summary of Work

The objectives articulated in Section 1.3 have been fulfilled. An extended kinematic model, based on the Volvo Transport Model (VTM) and verified against a previously validated model, has been developed to accommodate asymmetric left–right ride heights. Building on this foundation, air-spring and flow dynamics were incorporated to create a multi-body, heavy-vehicle, air-suspension model. This model serves as a platform for future development of control algorithms and research on vehicle dynamics.

A nonlinear two-track vehicle dynamics model was then formulated, including a nonlinear tire model, coupled yaw and roll dynamics, lateral weight transfer, and integrated air-spring behaviour. The model was used to design a Nonlinear Model Predictive Controller, which was implemented and evaluated against a Proportional-Integral (PI) controller across several scenarios with varying steering inputs and payload masses. The results show that the NMPC controller was effective in reducing the LTR and peak roll angles for non-alternating steer inputs, and in preventing rollover for a realistic driver input during a turn at high speed. However, limitations of the system for quick alternating steering inputs were also demonstrated, with a slightly higher LTR index and a slight increase in understeer behavior attributed to the pitch response. In conclusion, the NMPC demonstrates a safety improvement and the ability to prevent rollover events from occurring, albeit at the slight cost of reduced handling performance.

6.2 Future Work

The implemented air suspension model has not yet been validated against real-world data. As a result, its accuracy is currently assumed rather than verified. To further develop and rely on the model for control and simulation purposes, experimental validation is necessary.

To date, the controller has only been evaluated in a simulated environment, without consideration for real-time constraints. To extend this work toward practical implementation, it is necessary to significantly accelerate the controller and integrate it into a real-time control framework. Achieving real-time capability is a critical step in transitioning from purely simulation-based development to deployment on actual

hardware, which would be the ultimate goal.

The current vehicle model captures the coupled yaw–roll dynamics, which are essential for analysing lateral stability and rollover behaviour. However, it does not account for pitch motion or fully three-dimensional interactions between roll, pitch, and yaw. A natural extension of this work would be to develop a comprehensive vehicle dynamics model that incorporates pitch behavior. In this thesis, only flat road conditions were considered, incorporating pitch dynamics would enable more realistic simulations in the presence of slopes, road gradients, or vertical disturbances such as road bumps or pot holes.

Another avenue for future research is improving the response time of the air suspension system. In the current setup, the dynamics are limited by a maximum valve flow and component sizes. Investigating the use of larger or faster-acting valves could allow quicker pressure adjustments in the air suspensions, thereby enhancing the system's ability to counteract roll motion more effectively

Lastly, a potentially promising direction for future work would be the inclusion of additional actuators, specifically the braking system. Implementing braking into the NMPC framework would enable the NMPC to utilize air suspension not only to mitigate roll but also to apply braking torques to each individual wheel, allowing for more advanced control strategies.

Bibliography

[1] Swedish Parliament. Nollvisionen – ett etappmål för säker vägtrafik. Government policy decision, 1997. Adopted by the Swedish Parliament (Riksdagen), available from the Swedish Transport Administration (Trafikverket).

[2] Catherine A. Shaheed, Venkat K. Rao, Minh-Dang Vu, Elliott R. Haut, and Adil H. Haider. Rollover crashes: An underestimated danger. *Journal of Trauma Management & Outcomes*, 8(1):1–7, 2014.

[3] Mozhgan Nasr Azadani and Azzedine Boukerche. A novel multimodal vehicle path prediction method based on temporal convolutional networks. *IEEE Transactions on Intelligent Vehicles*, 2022.

[4] Volvo Group Trucks Technology. Volvo Truck Model, Simulink library, 2023. Developed at Volvo Group Trucks Technology.

[5] Volvo Trucks. VTM Plant Model Description, 2018. Unpublished internal company document.

[6] Cor-Jacques Kat and Pieter Schalk Els and. Interconnected air spring model. *Mathematical and Computer Modelling of Dynamical Systems*, 15(4):353–370, 2009.

[7] OpenAI. Image generated using DALL · E 3 via ChatGPT. `https://chat.openai.com`, 2025. Accessed June 16, 2025, via https://chat.openai.com.

[8] Andrew W. Peterson Yang Chen and Mehdi Ahmadian. Achieving anti-roll bar effect through air management in commercial vehicle pneumatic suspensions. *Vehicle System Dynamics*, 57(12):1775–1794, 2019.

[9] Carl-Philip Lartén. Modeling and identification of air suspension in heavy-duty vehicles. Master of science thesis in electrical engineering, Linköping University, SE-581 83 Linköping, Sweden, 2016. In cooperation with Scania CV AB, Stefan Sappei.

[10] A.J. Nieto, A.L. Morales, A. González, J.M. Chicharro, and P. Pintado. An analytical model of pneumatic suspensions based on an experimental characterization. *Journal of Sound and Vibration*, 313(1-2):290–307, 2008.

[11] Xiaohua Sun, Yujun Cai, Shuo Wang, et al. A hybrid approach to modeling and control of vehicle height for electronically controlled air suspension. *Chinese Journal of Mechanical Engineering*, 29:152–162, 2016.

[12] Brad Schofield. *Vehicle Dynamics Control for Rollover Prevention*. Licentiate thesis, Department of Automatic Control, Lund University, Lund, Sweden, 2006. Accessed: 2025-05-13.

[13] Hans B. Pacejka. *Tire and Vehicle Dynamics*. Butterworth-Heinemann, 3rd edition, 2012.

[14] Mike Blundell and Damian Harty. *The Multibody Systems Approach to Vehicle Dynamics*. Elsevier, Netherlands, 2 edition, 2014.

[15] Kristoffer Lundahl, Karl Berntorp, Björn Olofsson, Jan Åslund, and Lars Nielsen. Studying the influence of roll and pitch dynamics in optimal road-vehicle maneuvers. August 2013. 23rd International Symposium on Dynamics of Vehicles on Roads and Tracks ; Conference date: 19-08-2013.

[16] John Smith. Understanding control theory: Basics, applications, and types of controllers. *Journal of Electrical and Electronic Systems*, 12(4):1–5, 2023.

[17] Ylva Lindberg. A comparison between mpc and pid controllers for education and steam reformers. Master's thesis, Chalmers University of Technology, Gothenburg, Sweden, 2014.

[18] Mohammed Alhajeri and Masoud Soroush. Tuning guidelines for model-predictive control. *Industrial & Engineering Chemistry Research*, October 2021. Fourth revised version, submitted for publication.

[19] Lars Grüne and Jürgen Pannek. *Nonlinear Model Predictive Control: Theory and Algorithms*. Communications and Control Engineering. Springer International Publishing, 2nd edition, 2017.

[20] Liviu Gr. Ixaru and Guido Vanden Berghe. *Exponential Fitting*, volume 568 of *Mathematics and Its Applications*. Springer, 2004.

[21] Jasem Tamimi and Pu Li. Nonlinear model predictive control using multiple shooting combined with collocation on finite elements. In *7th IFAC International Symposium on Advanced Control of Chemical Processes (ADCHEM 2009)*, pages 703–708, 2009.

[22] Anders Hansson, Fredrik Magnusson, and Joel Andersson. fatrop: An nlp solver for real-time optimization with algorithmic differentiation and sparsity-exploiting linear algebra. *arXiv preprint arXiv:2303.16746*, 2023.

[23] Pavel Anistratov, Björn Olofsson, and Lars Nielsen. Lane-deviation penalty formulation and analysis for autonomous vehicle avoidance maneuvers. *Proceedings of the Institution of Mechanical Engineers, Part D: Journal of Automobile Engineering*, 235(12):3036–3050, 2021.

[24] Ernst Hairer and Gerhard Wanner. *Solving Ordinary Differential Equations II: Stiff and Differential-Algebraic Problems*, volume 14 of *Springer Series in Computational Mathematics*. Springer, 2nd revised edition, 1996.

[25] Bengt Lennartsson. *Reglerteknikens grunder*. Studentlitteratur, Lund, Sweden, 2 edition, 2002.

[26] Muniru Olajide Okelola, David Oluwagbemiga Aborisade, and Philip Adesola Adewuyi. Performance and configuration analysis of tracking time anti-windup pid controllers. *Jurnal Ilmiah Teknik Elektro Komputer dan Informatika*, 6(2):20–29, Jan. 2021.

[27] Kristoffer Lundahl, Chen Lee, Erik Frisk, and Lars Nielsen. Analyzing rollover indices for critical truck maneuvers. *Commercial Vehicles*, 8(1):189–196, 2015.

[28] Neha R. Dixit. Evaluation of vehicle understeer gradient definitions. Master of science thesis, Ohio State University, Columbus, OH, 2009. Advisor: Dennis Guenther, PhD. Committee Member: Gary Heydinger, PhD.

[29] Juliette Torinsson, Mats Jonasson, Derong Yang, and Bengt J.H. Jacobson. Upper bounds of lateral tire slip loss minimization during daily driving using

torque vectoring. https://research.chalmers.se/en/publication/537730, 2022. Preprint.

[30] Yasuyuki Tanabe, Yuichiro Minakuchi, Yoshinori Kono, Kyoichi Tagami, Masayoshi Kimura, and Hiroo Teruuchi. Study on roll angle control based on passenger comfort index. In *Proceedings of the 28th International Symposium on Advanced Vehicle Control (AVEC)*, Tochigi, Japan, 2025. Hitachi Astemo, Ltd. and Hitachi Astemo Europe GmbH, Springer.

[31] Transportstyrelsen. Lastbil – regler för personbil, lastbil och buss, n.d. Accessed: 2025-05-23.

A

State Trajectories and Control Inputs

A.1 Constant Turn

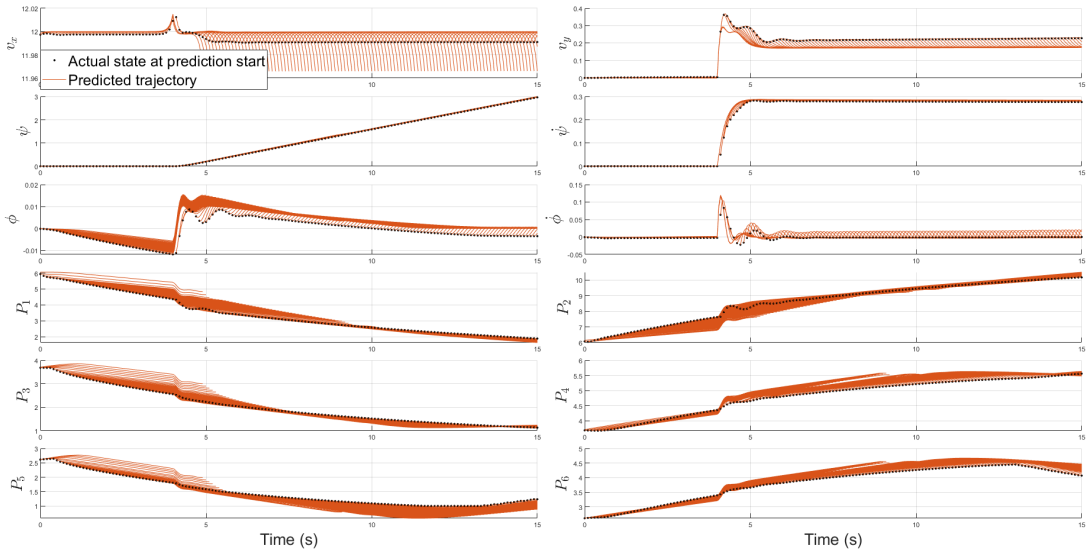

Figure A.1: NMPC State Trajectories, Constant Turn, 5 Ton Payload

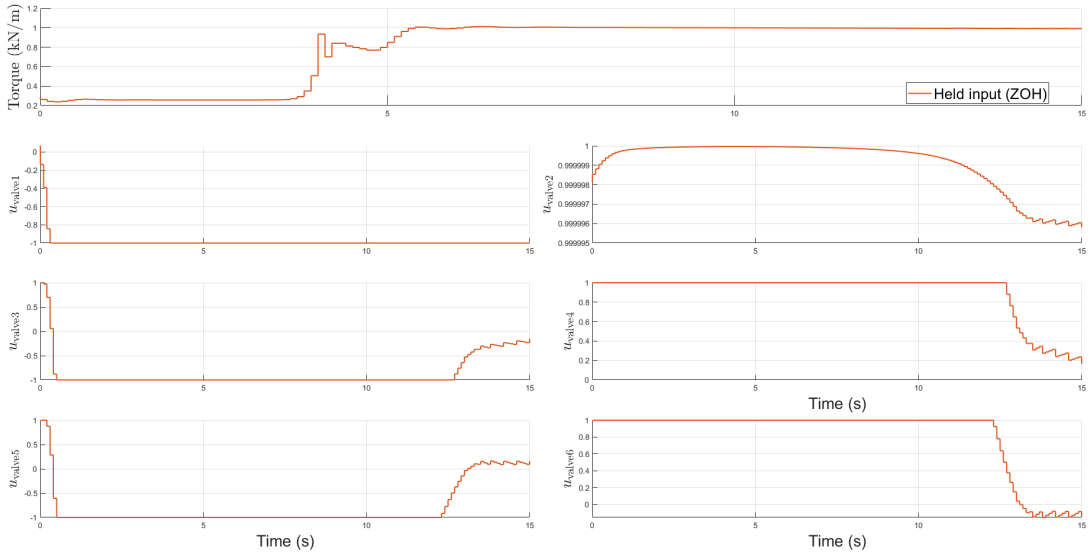

Figure A.2: NMPC Control Inputs, Constant Turn, 5 Ton Payload

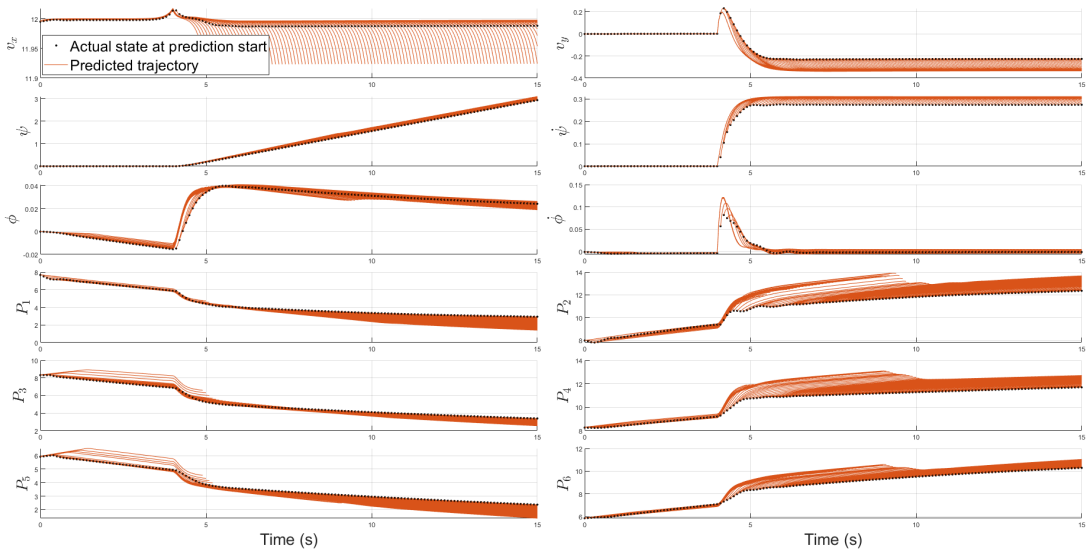

Figure A.3: NMPC State Trajectories, Constant Turn, Full Payload

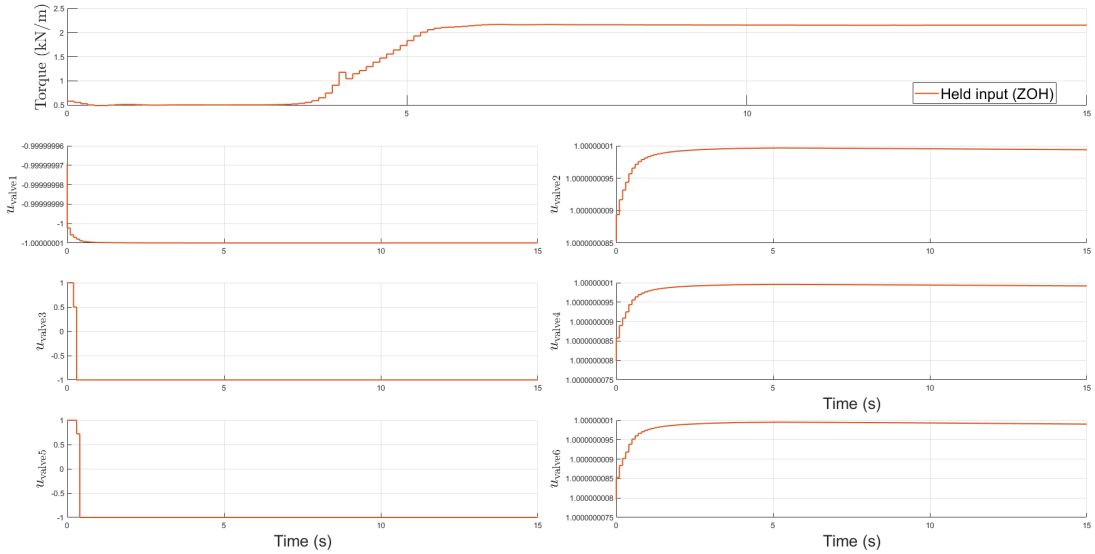

Figure A.4: NMPC Control Inputs, Constant Turn, Full Payload

A.2 Lane Change

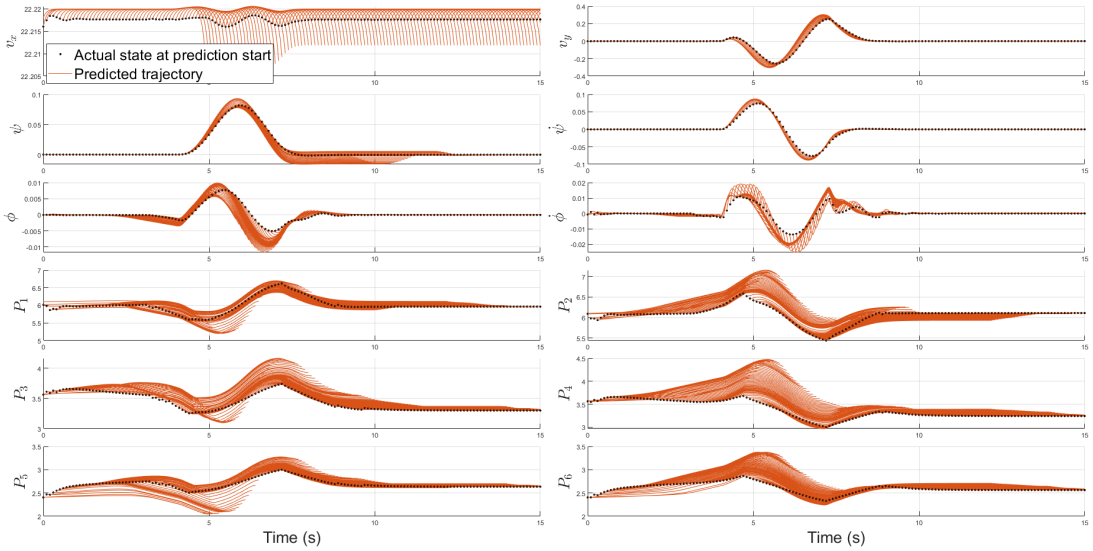

Figure A.5: NMPC State Trajectories, Lane Change, 5 Ton Payload

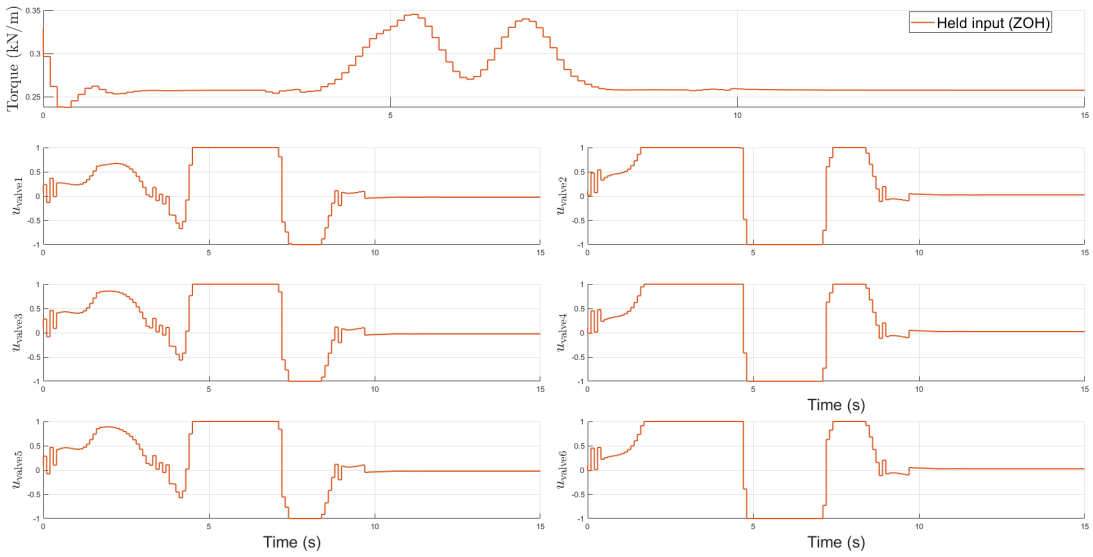

Figure A.6: NMPC Control Inputs, Lane Change, 5 Ton Payload

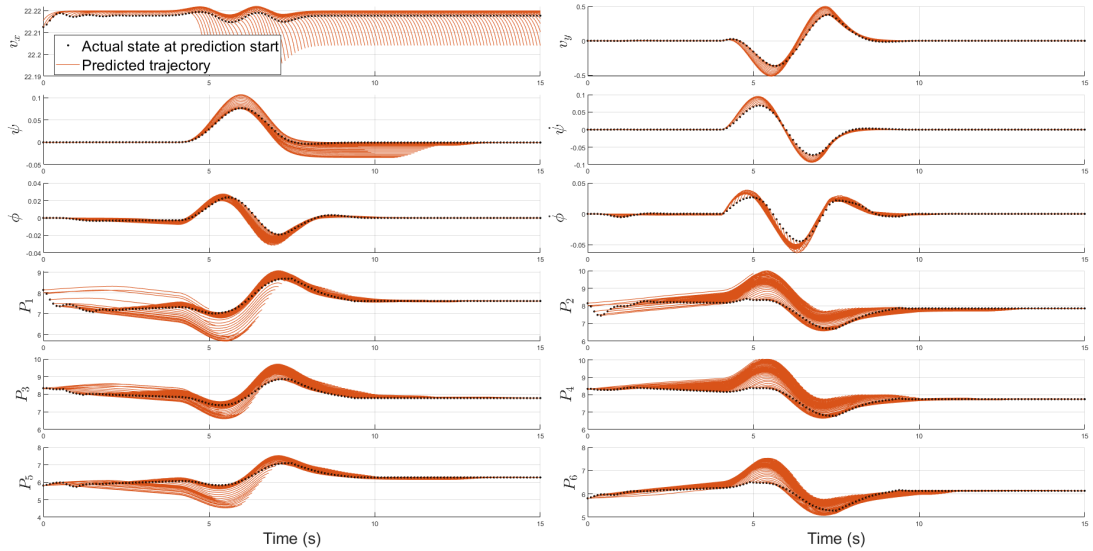

Figure A.7: NMPC State Trajectories, Lane Change, Full Payload

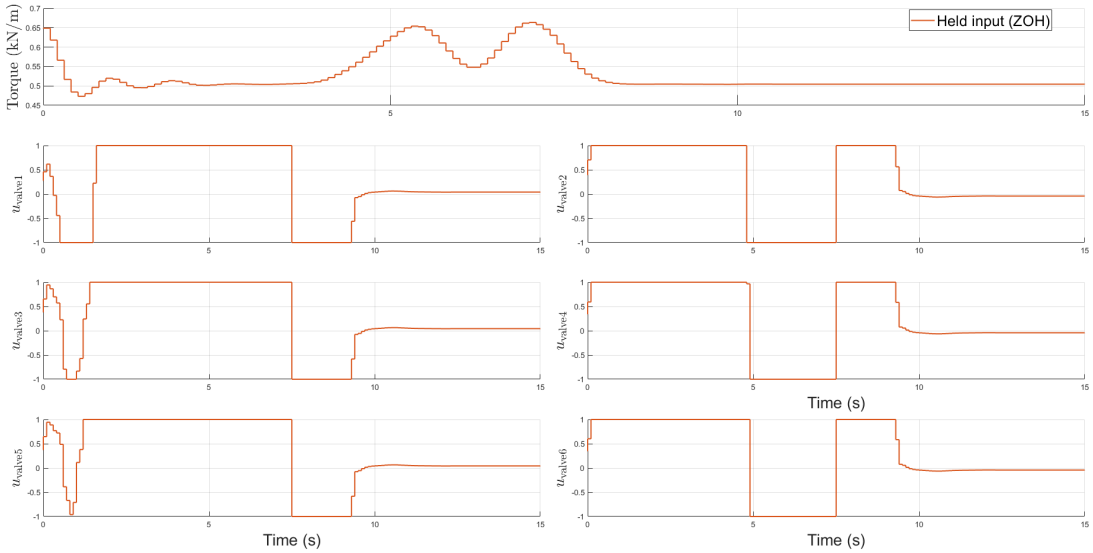

Figure A.8: NMPC Control Inputs, Lane Change, Full Payload

A.3 Ramp-Hold Steer

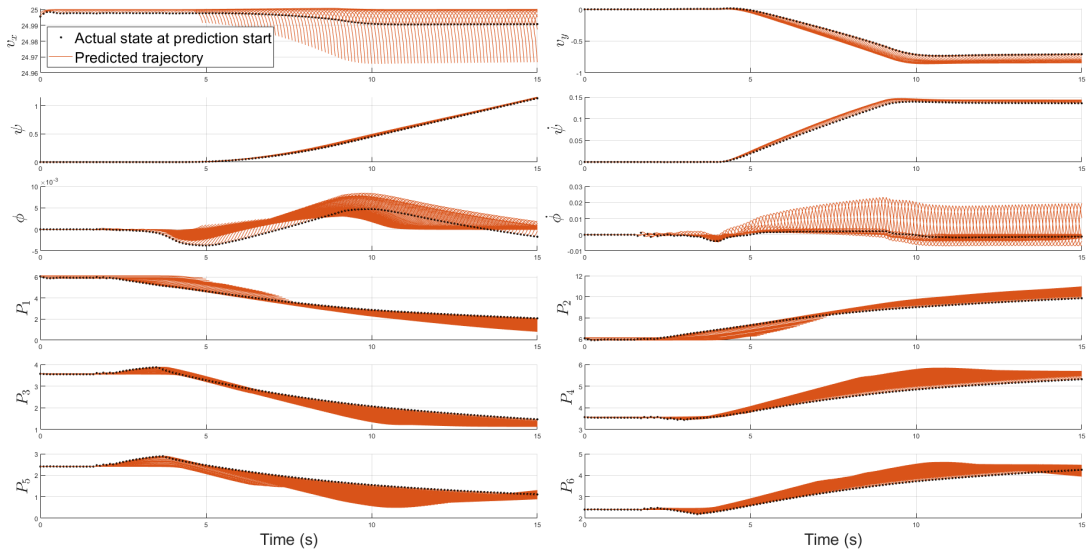

Figure A.9: NMPC State Trajectories, Ramp-Hold Steer, 5 Ton Payload

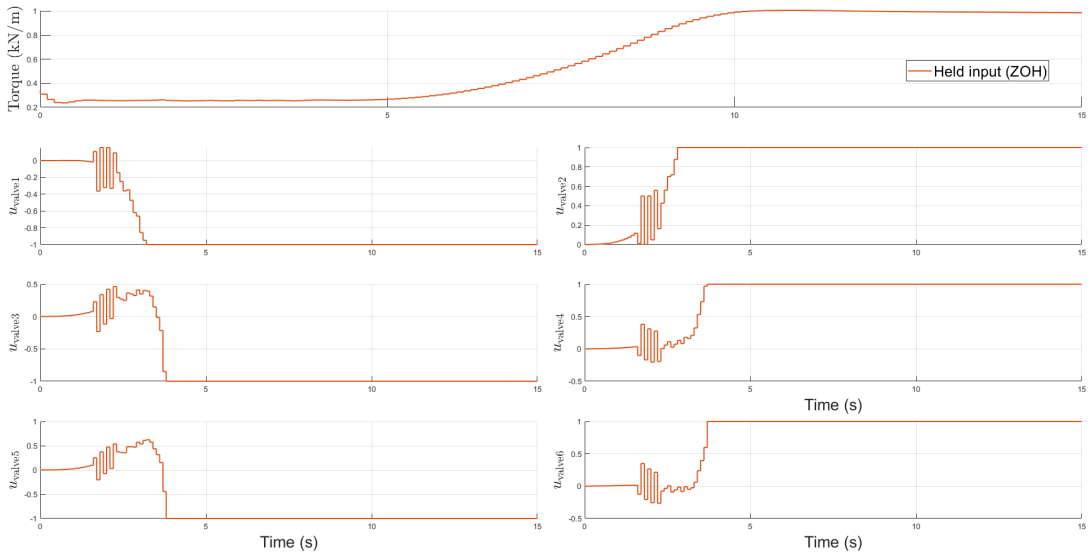

Figure A.10: NMPC Control Inputs, Ramp-Hold Steer, 5 Ton Payload

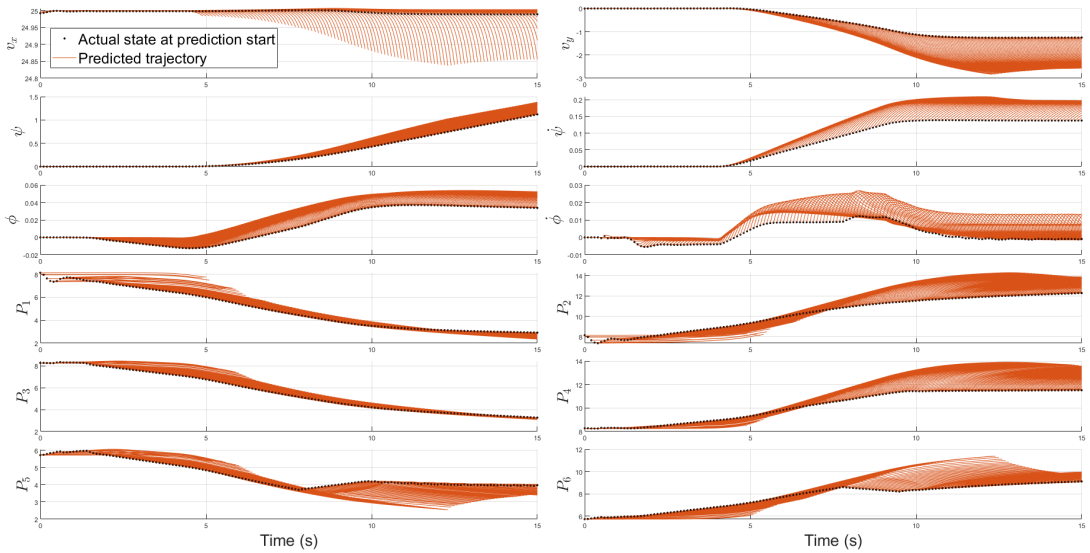

Figure A.11: NMPC State Trajectories, Ramp-Hold Steer, Full Payload

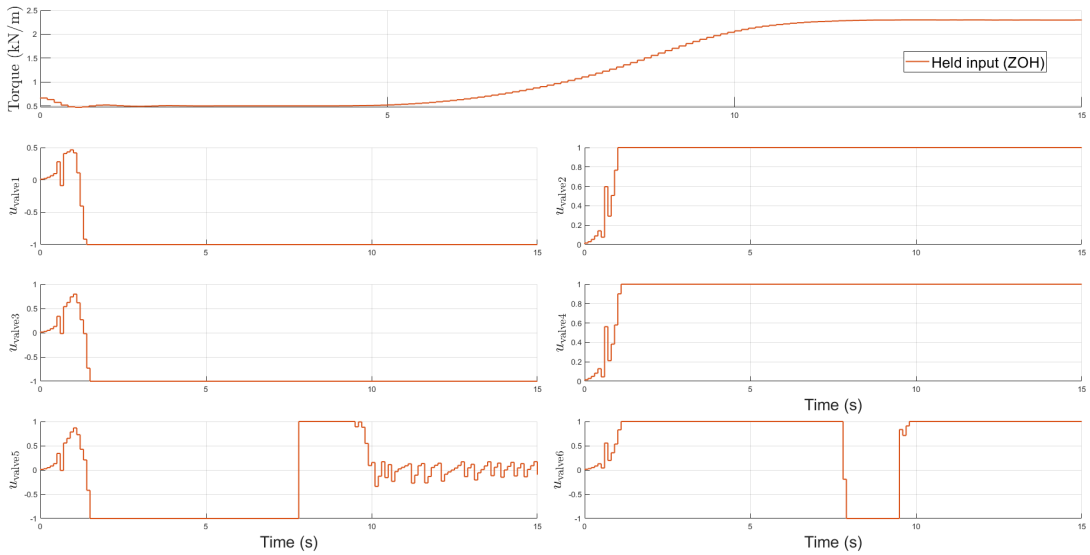

Figure A.12: NMPC Control Inputs, Ramp-Hold Steer, Full Payload

B

Simulation Pitch Response - Other Scenarios

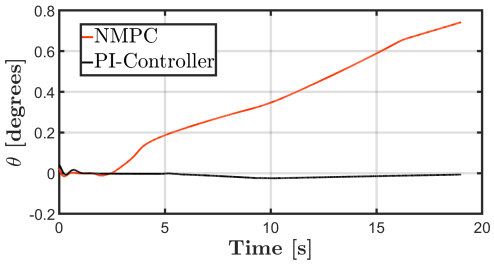

(a) 5 Ton Payload

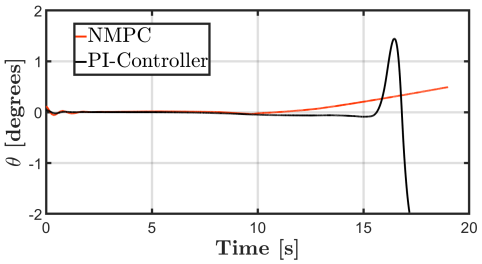

(b) Full 18.17 ton payload

Figure B.1: Pitch Response during Ramp-hold turn

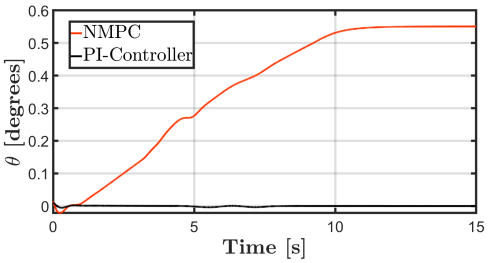

(a) 5 Ton Payload

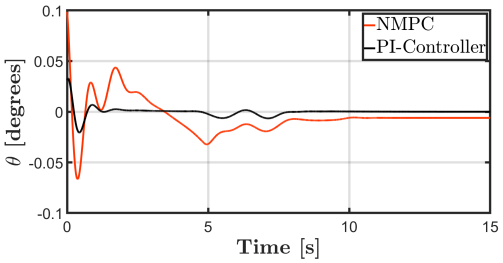

(b) Full 18.17 ton payload

Figure B.2: Pitch Response during lanechange maneuver

DEPARTMENT OF SOME SUBJECT OR TECHNOLOGY
CHALMERS UNIVERSITY OF TECHNOLOGY
Gothenburg, Sweden
www.chalmers.se

CHALMERS
UNIVERSITY OF TECHNOLOGY